Photostability Testing of FMT/RF With Radical Scavenger

FMT and RF were dissolved in 20 mM NaPB (pH 7.4). A mixture containing FMT (300 μM) and RF (2 μM) in a 5 mL clear glass vial was supplemented with radical scavengers (500 μM), including VC, Tyr, Trp, Cys, NaN_3, Na_2SO_3, His, BHT, and D-mannitol. Each sample was set in an Atlas Suntest CPS+ solar simulator and irradiated with simulated sunlight for 30 min. Each sample was diluted 100-fold, and the remaining FMT in the sample was measured by UPLC/ESI-MS analysis, as described in section *Photodegradation Profiles of FMT/RF.*

Pharmacokinetic Study

Animals

Male Sprague-Dawley rats (8-10 weeks of age; Japan SLC, Shizuoka, Japan), weighing 250-323 g, were housed 2 per cage in the laboratory with free access to food and water, and maintained on a 12-h dark/light cycle in a room with controlled temperature (24 ± 1°C) and humidity (55 ± 5%). All procedures used in the present study were conducted in accordance with the guidelines approved by the Institutional Animal Care and Ethical Committee of the University of Shizuoka and Yamanashi.

Plasma Concentration of FMT

Blood samples were obtained at a volume of 300 μL from the tail vein after the intravenous administration of FMT (1 mg/kg) containing RF (0.01 mg/kg) with or without VC (1 mg/kg) dissolved in saline at the indicated times (10, 20, 30 min, 1, 1.5, 2, 4, and 6 h). The blood samples were centrifuged at 10,000*g* for 10 min to prepare plasma samples, and the samples were kept frozen at below −20°C until they were analyzed. FMT concentrations in plasma were estimated by an internal standard method using UPLC/ESI-MS. Briefly, 250 μL of MeOH containing quinine (700 ng/mL; as internal standard) was added to 100 μL of plasma sample, followed by centrifugation at 10,000*g* for 10 min, and filtration at 0.22 μM. The concentration of FMT in the supernatant was analyzed by UPLC/ESI-MS, as described in section *Photodegradation Profiles of FMT/RF.* Analysis was also carried out using SIR for specific *m/z* 325.4 for quinine $[M+H]^+$. The pharmacokinetic parameters for FMT were calculated by two-compartmental methods using the WinNonlin® program (Ver. 4.1; Pharsight Corporation, Mountain View, CA).

Statistical Analysis

For statistical comparisons, one-way ANOVA with pairwise comparison by Fisher least significant difference procedure was used. A p value of less than 0.05 was considered significant for all analyses.

Results and Discussion

Photochemical Properties of FMT and RF

A photosensitizing drug can be excited by sunlight, composed of VIS (400-700 nm), UVA (320-400 nm), and part of UVB (290-320 nm).[18] The photo-excited drug may elicit photochemical reactions.[19] The UV-VIS absorption spectral measurement of such drugs has been commonly used as an immediate and simple method for predicting their photoreactivity.[20,21] The UV-VIS spectral patterns of FMT and RF were recorded in 20 mM NaPB (pH 7.4) (Fig. 2). RF showed strong absorption in the UVA-VIS range, and the lowest energy bands of RF had maxima at approximately 370 and 440 nm. The UV-VIS spectral patterns of RF overlapped with the sunlight spectrum. In contrast, the absorption of FMT in the UVA-VIS range was negligible. In theory, RF can thus absorb photon energy and be excited upon exposure to sunlight, whereas FMT does not have photoreactive potential.

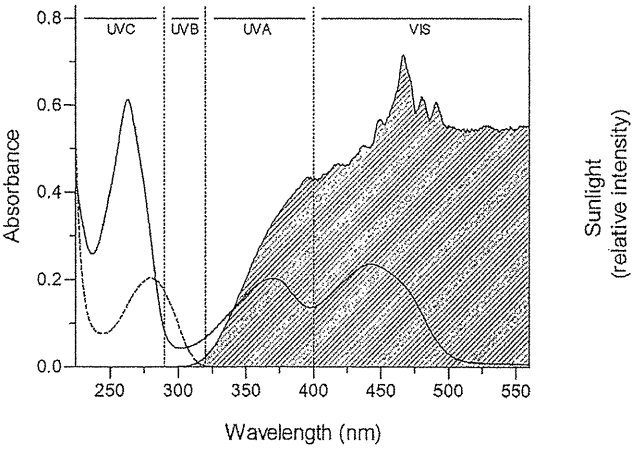

Figure 2. Average intensity of sunlight at the earth's surface and UV-VIS absorption spectra of RF and FMT in 20 mM NaPB (pH 7.4). RF, solid line; and FMT, broken line. Average intensity of sunlight (shaded) was taken from a previous report.[18]

The primary events in any photosensitization process can be the absorption of photon energy and subsequent generation of ROS: superoxide through electron or hydrogen transfer-mediated free radical generation (type I photochemical reaction), and singlet oxygen through energy transfer from an excited triplet photosensitizer to oxygen or biomolecules (type II photochemical reaction).[22] The ROS assay was designed for the photoreactivity assessment of pharmaceutical substances on the basis of ROS generation from photoirradiated compounds.[13] The ROS assay was carried out on both FMT and RF at a concentration of 50 μM (Fig. 3). For comparison, the ROS assay was also conducted for quinine, a typical phototoxic drug, as a positive control, and sulisobenzone, a sunscreen agent with no phototoxic potential, as a negative control, at the same concentration (50 μM). FMT and RF kept in the dark did not show any ROS generation (data not shown). The kinetics of ROS generation from irradiated RF indicated that superoxide was rapidly generated compared with singlet oxygen, suggesting that the exposure of RF under simulated sunlight (250 W/m^2) leads to the generation of ROS, mainly through a type I photochemical reaction in the early stage after irradiation. The exposure of RF to simulated sunlight for 1 h resulted in the generation of both singlet oxygen ($\Delta A_{440nm} \times 10^3$: 379.2 ± 8.7) and superoxide ($\Delta A_{560\ nm} \times 10^3$: 479.7 ± 16.1). In contrast, FMT exhibited negligible ROS generation [singlet oxygen ($\Delta A_{440\ nm} \times 10^3$): 5.7 ± 2.0; and superoxide ($\Delta A_{560\ nm} \times 10^3$): 7.2 ± 1.6] from FMT upon light exposure for 1 h. As observed in a previous study, sulisobenzone had no ability to yield ROS upon exposure to simulated sunlight. In contrast, the exposure of quinine to simulated sunlight for 1 h led to the generation of ROS [singlet oxygen ($\Delta A_{440\ nm} \times 10^3$): 196.6 ± 8.7; and superoxide ($aA_{560\ nm} \times 10^3$): 232.9 ± 5.5], and the ROS-generating ability of RF was higher than that of quinine at a concentration of 50 μM. According to the results from UV-VIS spectral analysis and ROS assay, RF had high photoreactive potential through type I and II photochemical reactions, possibly leading to the photodegradation of FMT/RF.

Photostability of FMT/RF

For further photochemical characterization, photostability testing was carried out for FMT (300 μM) with or without RF (2 μM)

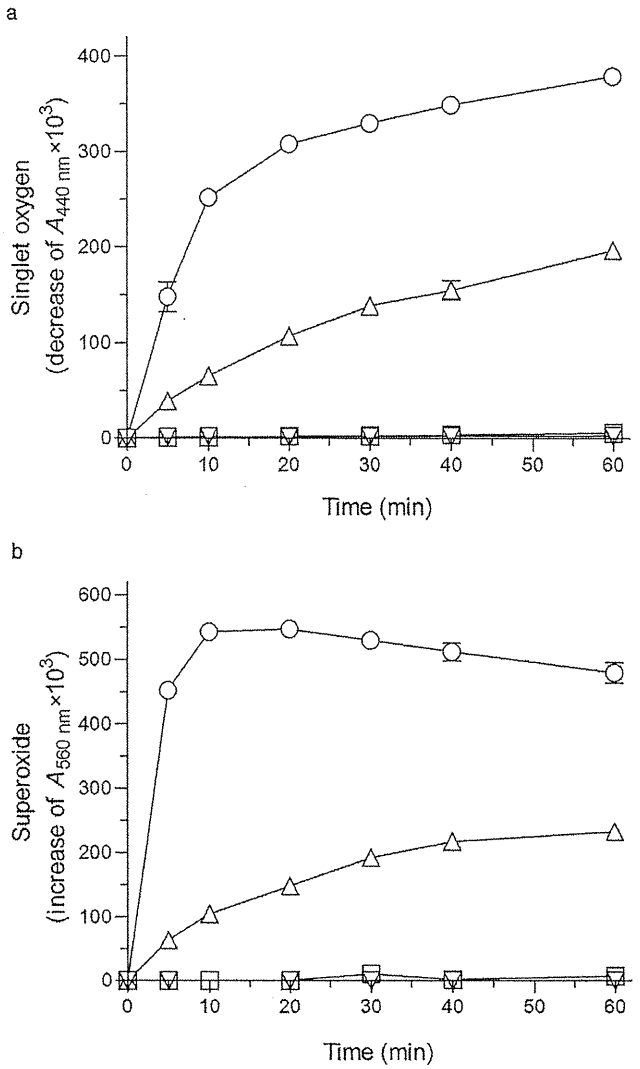

Figure 3. Generation of ROS from photoirradiated RF and FMT. Time course of singlet oxygen (a) and superoxide (b) generation from RF (50 μM) and FMT (50 μM) in 20mM NaPB (pH 7.4) exposed to simulated sunlight (250 W/m^2) for the indicated periods. ○, RF; □, FMT; Δ, quinine (50 μM, positive control); and ▽, sulisobenzone (50 μM, negative control). Data represent the mean ± SD of three experiments.

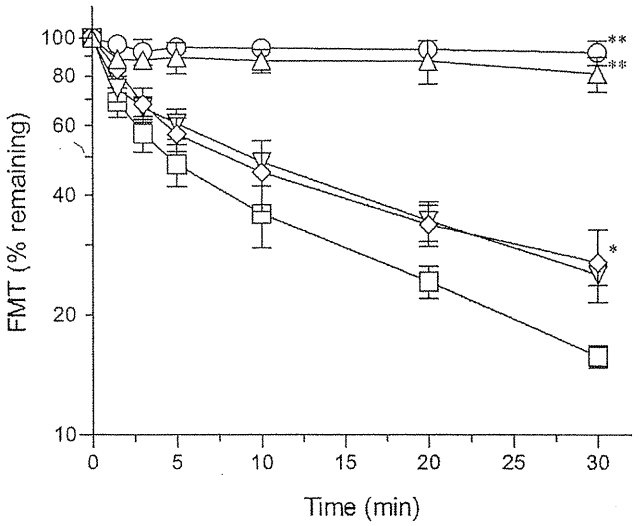

Figure 4. Photodegradation profile of FMT (300 μM) with or without RF (2 μM) and several radical scavengers in 20 mM NaPB (pH 7.4) irradiated with simulated sunlight (250 W/m^2). ○, FMT; □, FMT/RF; ▽, FMT/RF with NaN_3 (500 μM); Δ, FMT/RF with VC (500 μM); and ◊, FMT/RF with BHT (500 μM). Data represent the mean ± SD of three experiments. *, $p < 0.05$; and **, $p < 0.001$ with respect to FMT/RF at the same time point.

in 20 mM NaPB (pH 7.4) (Fig. 4). FMT and FMT/RF were exposed to the simulated sunlight (250 W/m^2) at 25°C for the indicated periods, and then subjected to UPLC/ESI-MS analysis. No samples kept in the dark showed any degradation for at least 30 min (data not shown). The exposure of FMT to the simulated sunlight for 30 min resulted in slight degradation of FMT potency (ca. 8%); however, the presence of RF accelerated the photodegradation of FMT, as evidenced by a ca. 84% reduction of FMT potency in FMT/RF. These findings might be consistent with the previous observation that FMT served as a ROS acceptor.[16]

In an attempt to evaluate the possible role of ROS in the photodegradation of FMT/RF, a series of experiments were performed in which several radical scavengers (500 μM) were included in FMT/RF solution during irradiation. The radical scavengers used were as follows: NaN_3, a singlet oxygen scavenger; BHT, a hydroxyl radical scavenger; and VC, a superoxide scavenger.[23] The addition of all radical scavengers led to a protective effect against the photodegradation of FMT/RF; in particular, VC showed ca. 86% attenuation of photodegradation (Fig. 4). A clear linear relationship was obtained according to the following equation: $\ln A = \ln A_0 - kt$ (apparent first-order kinetics), where A is the remaining peak area of FMT, k is the slope (degradation rate constant), and t is the time (min). The initial degradation rate constant ($k_{initial}$) for FMT/RF with VC was ca. 7-fold lower than that for FMT/RF alone (Table 1). These results were in agreement with the data from the ROS assay, suggesting that ROS from irradiated RF caused the photodegradation of FMT/RF, and a type I photochemical reaction might be mainly involved in the photodegradation pathway of FMT/RF.

Attenuating Effect of Radical Scavengers on the Photodegradation of FMT/RF

In general, the protection of photolabile drugs from light by using a film coating has been widely applied to avoid the photodegradation of drug under irradiation.[24] Light protection may also be a viable approach to improve the photostability of FMT/RF, although light protection using shading film might delay the identification of physicochemical incompatibility, including color change and precipitation. Thus, to improve the photostability of FMT/RF, differential approaches may be needed on the basis of the mechanisms of photodegradation of FMT/RF.

To develop a photochemically stabilized formulation of FMT, with the exposure of FMT/RF to various radical scavengers under

Table 1
Initial Degradation Rate Constants of Photodegradation for FMT With or Without RF and Radical Scavengers

Variable	$k_{initial}$ (min^{-1})
FMT (300 μM)	0.0176 ± 0.0170
FMT (300 μM)/RF (2 μM)	0.144 ± 0.0381
FMT/RF with NaN_3 (500 μM)	0.0959 ± 0.0322
VC (500 μM)	0.0203 ± 0.0223
BHT (500 μM)	0.112 ± 0.0206

$k_{initial}$, initial degradation rate constant (from $t = 0$ to 5 min after irradiation). Data represent the mean ± 95% confidence interval of three experiments.

simulated sunlight (250 W/m^2) for 30 min, the remaining FMT of each sample was determined by UPLC/ESI-MS analysis (Fig. 5). The radical scavengers used were as follows: (i) superoxide scavengers: VC, Tyr,[25] Trp,[25] and Cys[26]; (ii) singlet oxygen scavengers: Na_2SO_3,[27] NaN_3, and His; and (iii) hydroxyl radical scavengers: BHT and D-mannitol.[28] The addition of all test radical scavengers to FMT/RF tended to attenuate the photodegradation of FMT/RF. In particular, VC, Tyr, and Trp strongly inhibited the photodegradation of FMT/RF, and the remaining levels of FMT in FMT/RF with VC, Tyr, and Trp were found to be ca. 81%, 91%, and 88%, respectively. Thus, the addition of superoxide scavenger to FMT/RF could provide a protective effect against the photodegradation of FMT/RF.

However, FMT/RF with Tyr or Trp induced physicochemical incompatibility as indicated by a color change to a yellow-brown color. Namely, the oxidative reaction of Tyr and Trp caused the generation of yellow-colored products.[29] Furthermore, the accumulation of aromatic amino acids, including Tyr and Trp, in systemic circulation may increase the risk of hepatic encephalopathy in patients with liver failure.[30] VC exerts several functions, including the detoxification of exogenous compounds and cytochrome P-450 activity.[31] VC is also responsible for activating collagen proline hydroxylase in the conversion of proline to collagen hydroxyproline.[32] It plays a major role as an antioxidant and scavenger of ROS generated upon exposure to sunlight.[33] In addition, VC led to reductions in the incidence of most malignancies in humans.[31] In a clinical context, the maximum intravenous dose of VC was 2.8 g/day in humans[34]; thus, VC has high tolerability potential. From these attractive features, VC has been widely used as an ingredient of anti-aging cosmetic products and anti-cancer therapy drugs.[31,33] VC was also shown to have a photostabilizing effect on photosensitive drugs such as loratadine and pizotifen.[35] On the other hand, VC can also act as a pro-oxidant under a specific condition.[36] When Fe^{3+} is present, VC can convert Fe^{3+} into Fe^{2+}, which subsequently reacts with oxygen or hydrogen peroxide resulting in generation of ROS.[36] Herein, the pro-oxidative action of VC may affect VC-assisted photostabilization of FMT/RF. In the present study, Fe^{3+} was not added to test samples; thus, VC might play a role as an antioxidant. VC could be theoretically suitable for inhibiting the ROS-mediated photodegradation of FMT/RF in the absence of Fe^{3+}.

Pharmacokinetic Behavior of FMT

On the basis of the results from photostability testing, FMT/RF with VC (FMT/RF/VC) might be a viable photochemically stabilized FMT formulation. However, the addition of VC to FMT/RF may affect the pharmacokinetic behavior of FMT.

To prove bioequivalence between FMT/RF formulations with and without VC (1 mg/kg), pharmacokinetic study was carried out in rats after the intravenous administration of FMT (1 mg/kg) containing RF (0.01 mg/kg) with or without VC (1 mg/kg). Plasma concentration-time curves of FMT were obtained by UPLC/ESI-MS analysis after intravenous administrations of FMT/RF and FMT/RF/VC in rats (Fig. 6). The pharmacokinetic profile of FMT in the FMT/RF/VC group was likely to be similar to that in the FMT/RF group. The relevant pharmacokinetic parameters for intravenously administered FMT, including area under concentration versus time curve (AUC_{0-6}), distribution rate constant (k_a), and elimination rate constant (k_β), are listed in Table 2. The AUC_{0-6}, k_α, and k_β values in the FMT/RF/VC group were calculated to be 1.67 ± 0.22 μg·h/mL, 2.52 h^{-1}, and 4.67 h^{-1}, respectively. On the other hand, the AUC_{0-6}, k_α, and k_β values in the FMT/RF group were calculated to be 2.87 ± 0.44 μg·h/mL, 4.61 h^{-1}, and 4.76 h^{-1}, respectively. There were no significant differences in the pharmacokinetic parameters of FMT between the FMT/RF/VC and FMT/RF groups. Thus, the addition of VC to FMT/RF had no effects on the pharmacokinetic behavior of FMT in rats.

In general, drug-drug or drug-excipient interaction through direct and indirect pathways may affect the disposition and pharmacokinetic behavior of a drug, thereby affecting its safety and/or efficacy.[37,38] The administration of VC caused a rapid and pronounced decrease in the rate of excretion of sulfated metabolites of some drugs, including salicylamide and acetaminophen, in healthy adult volunteers.[39-41] In addition, VC has antioxidant activity, thereby affecting the radiosensitivity of radiosensitizing drugs such as metronidazole.[42] Thus, careful characterization of the physicochemical and pharmacokinetic properties is essential for the development of photochemically stabilized photolabile drug formulations by the addition of VC.

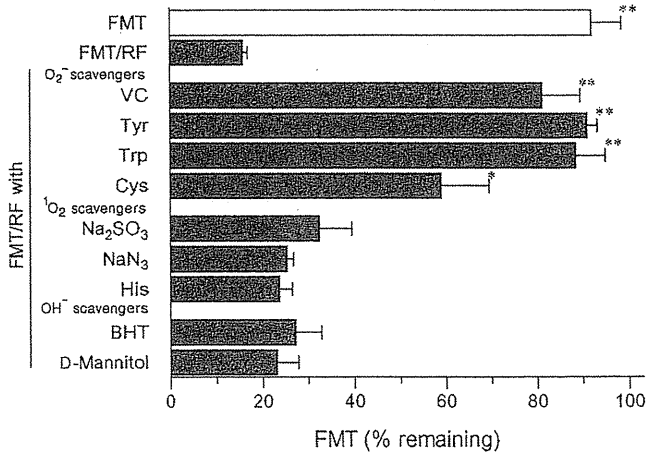

Figure 5. Photodegradation of FMT (300 μM) with RF (2 μM) and its attenuation by several scavengers (500 μM). Data represent the mean ± SD of three experiments. *, $p < 0.05$; and **, $p < 0.01$ with respect to FMT/RF.

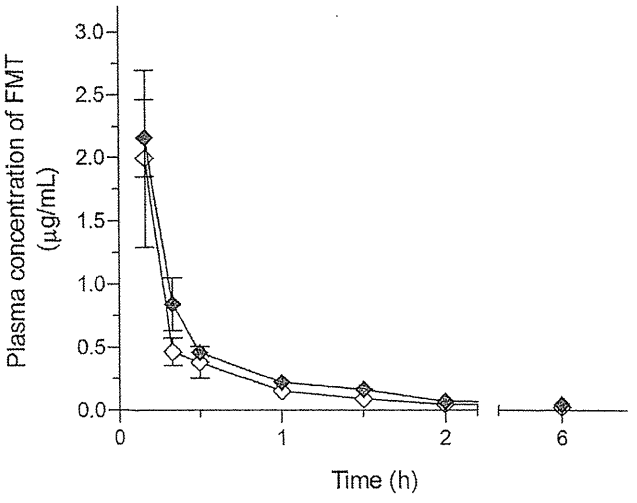

Figure 6. Plasma concentration–time profiles of FMT after intravenous administration of FMT (1 mg/kg) containing RF (0.01 mg/kg) with/without VC (1 mg/kg) in rats. ◊, FMT/RF; and ◆, FMT/RF/VC. Data represent the mean ± SE of four determinations.

Table 2
Pharmacokinetic Parameters of FMT After Intravenous Administration of FMT (1 mg/kg)/RF (0.01 mg/kg) With or Without VC (1 mg/kg)

Variable	k_α (h^{-1})	k_β (h^{-1})	AUC_{0-6} (μg-h/mL)
FMT/RF	4.61 (2.36-6.86)	4.76 (1.31-8.21)	2.87 ± 0.44
FMT/RF/VC	2.52 (1.61-3.43)	4.67 (3.25-6.09)	1.67 ± 0.22

k_α, distribution rate constant; k_β, elimination rate constant; and AUC_{0-6}, area under the curve of plasma concentration versus time from $t = 0$ to 6 h after administration. AUC_{0-6} represents the mean ± SE, and k_α and k_β represent the mean (95% confidence interval) of four determinations.

Conclusions

In the present study, the mechanism of the photodegradation of FMT/RF was partly deduced. According to UV-VIS spectral analysis, ROS assay, and photostability testing, RF had high photoreactive potential, and ROS generation from irradiated RF was involved in the photodegradation pathway of FMT/RF. The addition of VC to FMT/RF could improve the photostability of FMT/RF, and it had a negligible effect on the pharmacokinetic behavior of FMT. From these findings, the complementary use of VC would be a viable approach to improve the photostability of photolabile drugs, and it might provide reliable and consistent medication for the clinical use of photolabile drugs.

Acknowledgments

The authors are grateful to Ms. Yukiko Suzuki, Department of Pharmacokinetics and Pharmacodynamics, University of Shizuoka, for excellent technical assistance throughout this work.

References

1. Summa-Sorgini C, Fernandes V, Lubchansky S, Mehta S, Hallett D, Bailie T, Lapinsky SE, Burry L. Errors associated with IV infusions in critical care. *Can J Hosp Pharm.* 2012;65:19-26.
2. Vijayakumar A, Sharon EV, Teena J, Nobil S, Nazeer I. A clinical study on drug-related problems associated with intravenous drug administration. *J Basic Clin Pharm.* 2014;5:49-53.
3. Foinard A, Décaudin B, Barthélémy C, Debaene B, Odou P. Impact of physical incompatibility on drug mass flow rates: Example of furosemide-midazolam. *Ann Intensive Care.* 2012;2:28.
4. Kanji S, Lam J, Johanson C, Singh A, Goddard R, Fairbairn J, Lloyd T, Monsour D, Kakal J. Systematic review of physical and chemical compatibility of commonly used medications administered by continuous infusion in intensive care units. *Crit Care Med.* 2010;38:1890-1898.
5. Torosian MH. *Stability and compatibility issues. In Nutrition for the hospitalized patient: Basic science and principles of practice.* New York: Marcel Dekker; 1995:284.
6. Keyi X, Gagnon N, Bisson C, Desmarais M, LeBel M. Stability of famotidine in polyvinyl chloride minibags and polypropylene syringes and compatibility of famotidine with selected drugs. *Ann Pharmacother.* 1993;27:422-426.
7. Ichikawa E, Kimura M, Mori H, Yamazaki F, Hirano K. Apparent increase of insulin peak area in HPLC analysis of a preparation consisting of a mixture of insulin and total parenteral nutrition. *Chem Pharm Bull.* 2006;54:1196-1199.
8. DeRitter E. Vitamins in pharmaceutical formulations. *J Pharm Sci.* 1982;71:1073-1096.
9. Shen L, Ji HF, Zhang HY. Computational note on the photosensitization mechanisms of riboflavin. *J Mol Struct.* 2007;821:171-172.
10. Reynoso E, Spesia MB, Garcia NA, Biasutti MA, Criado S. Riboflavin-sensitized photooxidation of Ceftriaxone and Cefotaxime. Kinetic study and effect on *Staphylococcus aureus*. *J Photochem Photobiol B.* 2015;142:35-42.
11. Massad WA, Bertolotti S, Garcia NA. Kinetics and mechanism of the vitamin B_2-sensitized photooxidation of isoproterenol. *Photochem Photobiol.* 2004;79:428-433.
12. Scurachio RS, Skibsted LH, Metzker G, Cardoso DR. Photodegradation of folate sensitized by riboflavin. *Photochem Photobiol.* 2011;87:840-845.
13. Onoue S, Tsuda Y. Analytical studies on the prediction of photosensitive/phototoxic potential of pharmaceutical substances. *Pharm Res.* 2006;23:156-164.
14. Jaimini M, Rana AC, Tanwar YS. Formulation and evaluation of famotidine floating tablets. *Curr Drug Deliv.* 2007;4:51-55.
15. Rahman N, Kashif M. Kinetic spectrophotometric determination of famotidine in commercial dosage forms. *Anal Sci.* 2003;19:907-911.
16. Kurt A, Isaoglu U, Yilmaz M, Calik M, Polat B, Hakan H, Ingec M, Suleyman H. Biochemical and histological investigation of famotidine effect on postischemic reperfusion injury in the rat ovary. *J Pediatr Surg.* 2011;46:1817-1823.
17. Seto Y, Kato M, Yamada S, Onoue S. Development of micellar reactive oxygen species assay for photosafety evaluation of poorly water-soluble chemicals. *Toxicol In Vitro.* 2013;27:1838-1846.
18. Jagger J. *Why solar-ultraviolet photobiology? In Solar-UV actions on living cells.* New York: Praeger Scientific; 1985:1-10.
19. Moore DE. Drug-induced cutaneous photosensitivity: Incidence, mechanism, prevention and management. *Drug Saf.* 2002;25:345-372.
20. Henry B, Foti C, Alsante K. Can light absorption and photostability data be used to assess the photosafety risks in patients for a new drug molecule? *J Photochem Photobiol B.* 2009;96:57-62.
21. Onoue S, Igarashi N, Yamauchi Y, Murase N, Zhou Y, Kojima T, Yamada S, Tsuda Y. In vitro phototoxicity of dihydropyridine derivatives: A photochemical and photobiological study. *Eur J Pharm Sci.* 2008;33:262-270.
22. Onoue S, Seto Y, Gandy G, Yamada S. Drug-induced phototoxicity; an early in vitro identification of phototoxic potential of new drug entities in drug discovery and development. *Curr Drug Saf.* 2009;4:123-136.
23. Béchard SR, Quraishi O, Kwong E. Film coating: Effect of titanium dioxide concentration and film thickness on the photostability of nifedipine. *Int J Pharm.* 1992;87:133-139.
24. Lu CY, Liu YY. Electron transfer oxidation of tryptophan and tyrosine by triplet states and oxidized radicals of flavin sensitizers: A laser flash photolysis study. *Biochim Biophys Acta.* 2002;1571:71-76.
25. Devasagayam TP, Sundquist AR, Di Mascio P, Kaiser S, Sies H. Activity of thiols as singlet molecular oxygen quenchers. *J Photochem Photobiol B.* 1991;9:105-116.
26. Suzuki Y, Miura T, Ogiso T. Riboflavin photosensitized hemolysis of rat erythrocytes in the presence of serum. *J Pharmacobiodyn.* 1982;5:568-575.
27. Desesso JM, Scialli AR, Goeringer GC. d-Mannitol, a specific hydroxyl free radical scavenger, reduces the developmental toxicity of hydroxyurea in rabbits. *Teratology.* 1994;49:248-259.
28. Girotti AW. Photodynamic lipid peroxidation in biological systems. *Photochem Photobiol.* 1990;51:497-509.
29. Dyer JM, Bringans SD, Bryson WG. Characterisation of photo-oxidation products within photoyellowed wool proteins: Tryptophan and tyrosine derived chromophores. *Photochem Photobiol Sci.* 2006;5:698-706.
30. Dejong CH, van de Poll MC, Soeters PB, Jalan R, Olde Damink SW. Aromatic amino acid metabolism during liver failure. *J Nutr.* 2007;137:1579-1585.
31. Block G. Epidemiologic evidence regarding vitamin C and cancer. *Am J Clin Nutr.* 1991;54:1310-1314.
32. Barnes MJ. Function of ascorbic acid in collagen metabolism. *Ann NY Acad Sci.* 1975;258:264-277.
33. Ahmad I, Sheraz MA, Ahmed S, Shaikh RH, Vaid FH, ur Rehman Khattak S, Ansari SA. Photostability and interaction of ascorbic acid in cream formulations. *AAPS PharmSciTech.* 2011;12:917-923.
34. Japan Pharmaceutical Excipients Council. *Japanese Pharmaceutical Excipients Directory.* Tokyo: YAKUJINIPPO; 2000:6.
35. Abounassif MA, El-Obeid HA, Gadkariem EA. Stability studies on some benzocycloheptane antihistaminic agents. *J Pharm Biomed Anal.* 2005;36:1011-1018.
36. Rietjens IM, Boersma MG, Haan Ld, Spenkelink B, Awad HM, Cnubben NH, van Zanden JJ, Woude Hv, Alink GM, Koeman JH. The pro-oxidant chemistry of the natural antioxidants vitamin C, vitamin E, carotenoids and flavonoids. *Environ Toxicol Pharmacol.* 2002;11:321-333.
37. Buggins TR, Dickinson PA, Taylor G. The effects of pharmaceutical excipients on drug disposition. *Adv Drug Deliv Rev.* 2007;59:1482-1503.
38. Li W, Zeng S, Yu LS, Zhou Q. Pharmacokinetic drug interaction profile of omeprazole with adverse consequences and clinical risk management. *Ther Clin Risk Manag.* 2013;9:259-271.
39. Houston JB, Levy G. Modification of drug biotransformation by vitamin C in man. *Nature.* 1975;255:78-79.
40. Houston JB, Levy G. Drug biotransformation interactions in man VI: Acetaminophen and ascorbic acid. *J Pharm Sci.* 1976;65:1218-1221.
41. Houston JB, Levy G. Effect of route of administration on competitive drug biotransformation interaction: Salicylamide-ascorbic acid interaction in rats. *J Pharmacol Exp Ther.* 1976;198:284-294.
42. DiPalma JA, McMichael R. The interaction of vitamins with cancer chemotherapy. *CA Cancer J Clin.* 1979;29:280-286.

Pharm Res
DOI 10.1007/s11095-016-1887-3

RESEARCH PAPER

Development of an Improved Inhalable Powder Formulation of Pirfenidone by Spray-Drying: *In Vitro* Characterization and Pharmacokinetic Profiling

Yoshiki Seto[1] · Gen Suzuki[1] · Sharon Shui Yee Leung[2] · Hak-Kim Chan[2] · Satomi Onoue[1]

Received: 17 December 2015 / Accepted: 16 February 2016

ABSTRACT

Purpose Previously, a respirable powder (RP) formulation of pirfenidone (PFD) was developed for reducing phototoxic risk; however, PFD-RP demonstrated unacceptable *in vitro* inhalation performance. The present study aimed to develop a new RP system of PFD with favorable inhalation properties by spray-drying method.

Methods Spray-dried PFD (SD/PFD) was prepared by spray-drying with L-leucine, and the physicochemical properties and efficacy in an antigen-sensitized airway inflammation model were assessed. A pharmacokinetic study was also conducted after intratracheal and oral administration of PFD formulations.

Results Regarding powder characterization, SD/PFD had dimpled surface with the mean diameter of 1.793 μm. In next generation impactor analysis, SD/PFD demonstrated high *in vitro* inhalation performance without the need of carrier particles, and the fine particle fraction of SD/PFD was calculated to be 62.4%. Insufflated SD/PFD (0.3 mg-PFD/rat) attenuated antigen-evoked inflammatory events in the lung, including infiltration of inflammatory cells and myeloperoxidase activity. Systemic exposure level of PFD after insufflation of SD/PFD at the pharmacologically effective dose was 600-fold lower than that after oral administration of PFD at the phototoxic dose.

Conclusion SD/PFD would be suitable for inhalation, and the utilization of an RP system with SD/PFD would provide a safer medication compared with oral administration of PFD.

KEY WORDS inhalation · pirfenidone · pulmonary fibrosis · spray dry · systemic exposure

ABBREVIATIONS

$AUC_{0\text{-}inf}$	Area under the concentration *versus* time curve
BALF	Bronchoalveolar lavage fluid
C_{max}	Maximum concentration
EF	Emitted fraction
FPF	Fine particle fraction
HPLC	High performance liquid chromatography
ICH	The International Council on Harmonisation of Technical Requirements for Registration of Pharmaceuticals for human use
IPF	Idiopathic pulmonary fibrosis
MPO	Myeloperoxidase
MRT	Mean residence time
NGI	Next generation impactor
OVA	Ovalbumin
OVA-RP	Respirable powder formulation of ovalbumin
PBS	Phosphate buffered saline
PFD	Pirfenidone
PFD-RP	Respirable powder formulation of pirfenidone
RP	Respirable powder
SD/PFD	Spray-dried pirfenidone
SEM	Scanning electron microscopy
$t_{1/2}$	Elimination half-life
TMBZ	3,3′,5,5′-tetramethylbenzidine
UPLC/ESI-MS	Ultra-performance liquid chromatography equipped with electrospray ionization mass spectrometry
VMD	Volume median diameter

Electronic supplementary material The online version of this article (doi:10.1007/s11095-016-1887-3) contains supplementary material, which is available to authorized users.

✉ Satomi Onoue
onoue@u-shizuoka-ken.ac.jp

[1] Department of Pharmacokinetics and Pharmacodynamics, School of Pharmaceutical Sciences, University of Shizuoka, 52-1 Yada, Suruga-ku, Shizuoka 422-8526, Japan

[2] Advanced Drug Delivery Group, Faculty of Pharmacy University of Sydney, Sydney, NSW 2006, Australia

Published online: 14 March 2016

INTRODUCTION

Pirfenidone (PFD), 5-methyl-1-phenylpyridin-2-one, has been shown to have anti-inflammatory and anti-fibrotic properties and to suppress the progression of fibrotic and inflammatory events in the lung, liver, and kidney in experimental animal models (1–4). Potential mechanisms for the suppression of fibrogenesis by PFD have been reported, including the regulation of inflammatory cytokines and growth factors, attenuation of fibroblast proliferation, and inhibition of collagen synthesis (5), and together, these functions may mediate the anti-fibrotic effect of PFD. In clinical settings, PFD is the first orally-administered agent (Esbriet® or Pirespa®) for treating idiopathic pulmonary fibrosis (IPF) in Europe, Japan, India, and China (1,6,7). On the other hand, orally-administered PFD often causes systemic side effects, such as phototoxic skin reactions, gastrointestinal discomfort, and liver dysfunction (6,8,9). In particular, the incidence of phototoxic skin reactions after oral administration of PFD was reported to be over 50% in clinical trial (8). The mechanism of PFD-induced phototoxicity was partially identified in the previous investigation (10) and was attributed to high skin exposure levels of PFD. The International Council on Harmonisation of Technical Requirements for Registration of Pharmaceuticals for Human Use (ICH) guideline S10 (11) describes distribution of a chemical to light-exposed tissues as a critical characteristic for induction of phototoxic events; therefore, modulating the dermal distribution of PFD would reduce the phototoxic risk of PFD in the skin.

Recently, several inhalable formulation systems have been developed for treating respiratory inflammation, and insufflated formulations have been shown to achieve a high lung concentration and low systemic exposure of the drug (12,13). Hence, use of an inhalation system would be a suitable approach for developing PFD medication with a wide safety margin. A respirable powder (RP) formulation of PFD (PFD-RP) was previously developed for reducing phototoxic risk of PFD (14). Insufflated PFD-RP (0.3 mg-PFD/rat) attenuated inflammatory events in an antigen-evoked lung inflammation model and exhibited dramatically lower systemic exposure and skin distribution compared with orally-administered PFD at a phototoxic dose. Although PFD-RP would be useful for treatment of IPF with low phototoxic risk, drawbacks remain regarding its inhalation properties. In the previous investigation, PFD was micronized by jet-milling system, and PFD-RP was prepared with the use of lactose carriers. PFD-RP demonstrated fine dispersion and aerosolization of the jet-milled PFD powders. However, *in vitro* inhalation performance of PFD-RP analyzed by cascade impactor was unacceptable because the calculated fine particle fraction (FPF) value of PFD-RP was 23.4%. The slightly larger particle size of the jet-milled PFD may result in low treatment efficacy in clinical use. The particle size of a drug influences lung deposition; thus, reducing the size of PFD microparticles may be an appropriate approach to optimize the inhalation performance of a respirable formulation of PFD.

The spray-drying technique is widely used for preparing respirable microparticles with adequate inhalation properties (15,16), and this technology has been used for the production of inhalable dry powders for antibiotics (17–19), non-steroidal anti-inflammatory drugs (20), and immune suppressors (21). Therefore, the spray-drying technique may be suitable for preparing PFD microparticles with favorable inhalation performance. The aim of the present study was to produce a new inhalable powder formulation of PFD with favorable inhalation properties. Spray-dried PFD (SD/PFD) particles were obtained by spray-drying with L-leucine because the addition of L-leucine was shown to significantly increased FPF of a formulation with high dispersibility and flowability (22). The physicochemical characterization of SD/PFD was performed with respect to morphology, particle size distribution, and *in vitro* inhalation performance, and the pharmacological effects of insufflated SD/PFD were assessed using an experimental lung inflammation model. To verify the risk of side effects, the plasma concentration of PFD after intratracheal administration of SD/PFD was assessed by ultra-performance liquid chromatography equipped with electrospray ionization mass spectrometry (UPLC/ESI-MS), and the systemic exposure of PFD after intratracheal administration of SD/PFD was compared with that after oral administration of PFD at both non-phototoxic and phototoxic doses.

MATERIALS AND METHODS

Chemicals

PFD was kindly provided by Shionogi (Osaka, Japan). L-leucine was purchased from Sigma–Aldrich (New South Wales, Australia). Ammonium acetate, antipyrine, and trypan blue were bought from Wako Pure Chemical Industries (Osaka, Japan). Aluminum hydroxide gel, horseradish peroxidase, lactose, ovalbumin (OVA), and sodium pentobarbital were purchased from Sigma-Aldrich (St. Louis, MO, USA). Acetonitrile and 3,3′,5,5′-tetramethylbenzidine (TMBZ) were obtained from Honeywell International (Morristown, NJ, USA) and Dojindo Laboratories (Kumamoto, Japan), respectively. All other regents were obtained from commercial sources.

Powder Preparation

PFD and L-leucine were dissolved in water containing 30% ethanol at a weight ratio of 90:10, with a total solid content of 10 mg/ml. SD/PFD was prepared by spray-drying of the solution using a Buchi 290 spray dryer under open-loop

conditions using dehumidified air (Buchi Dehumidifier B-296) as the drying gas at a solution feed rate of 2 mL/min, aspiration rate of 38 m^3/h, and atomization rate of 819 NL/h. The inlet and outlet temperatures were 60 and 43°C, respectively. Spray-dried powders were stored in a desiccator containing silica gel at 20 ± 3°C until used.

Scanning Electron Microscopy (SEM)

Representative scanning electron microscopic images of SD/PFD were taken using Hitachi S-4500 FESEM (Hitachi, Tokyo, Japan) with approximately 15 nm gold coating. For the scanning electron microscopic observation, SD/PFD was fixed on an aluminum sample holder using double-sided carbon sticky tape.

Particle Size Distribution

The particle size distribution of SD/PFD was measured by laser diffraction using a Mastersizer 2000 (Malvern Instruments, UK). The real and imaginary refractive indices were set to 1.59 and 0.1, respectively. The dispersant (air) refractive index was set to 1.000. The powders were dispersed through the measurement window with compressed air at 1 bar and 3.5 bar for the spray freeze dry and spray dry formulations, respectively, using a Scirocco 2000 dry powder module (Malvern Instruments, UK). All measurements were performed in triplicate. Size was expressed by the volume median diameter (VMD) and width was defined as [D(*v*, 90)–D(*v*, 10)]/ D(*v*, 50), where D(*v*, 10), D(*v*, 50), and D(*v*, 90) were the equivalent volume diameters at 10, 50, and 90% cumulative volumes, respectively.

In Vitro Inhalation Performance

The *in vitro* inhalation performance of SD/PFD was assessed by dispersing 5 mg of SD/PFD into a Next Generation Impactor (NGI) at 100 L/min for 2.4 s using an Osmohaler™. Size 3 hydroxypropyl methylcellulose capsules (Capsugel, New South Wales, Australia) were used for powder loading. All dispersion experiments were conducted in triplicate (n = 3). The impactor stages were coated with silicon grease (Slipicone®; DC Products, Victoria, Australia) before testing to minimize particle bounce. After dispersion, the powder deposited on the capsule, inhaler, adaptor, and NGI stages were exhaustively washed with 3 ml 70% methanol–water mixture. Drug content at each location was quantified using a high performance liquid chromatography (HPLC) system from Shimadzu Corporation (Kyoto, Japan) and a NovaPak C18 column (4 μm, 3.9 × 150 mm; Waters, USA). The mobile phase was a mixture of methanol (50%) and water (50%, pH adjusted to 4.5 using orthophosphate acid). UV absorbance at a wavelength of 324 nm was used to detect PFD. The flow rate was 1 mL/min and the retention time for PFD was 2.5 min. The calibration curves were linear in the concentration range of 0.05–1 mg/mL ($R^2 = 0.999$, $n = 3$).

The lower cutoff diameters of NGI stages 1–7 at 100 L/min were 6.12, 3.42, 2.18, 1.31, 0.72, 0.40, and 0.24 μm, calculated by adjustment equations given in Appendix XII C of the British Pharmacopoeia (2011). The emitted fraction (EF) was the total amount of powder that exited the inhaler with respect to the recovered dose. The FPF was defined as the mass fraction of particles ≤ 5.0 μm with respect to the emitted dose. The cumulative fraction of particles with aerodynamic diameter ≤ 5.0 μm, corresponding to the FPF, was determined by interpolation.

In Vivo Preparations

Male Sprague–Dawley rats at 9–12 weeks of age (260–470 g body weight) were purchased from SLC Inc. (Hamamatsu, Japan), housed in the laboratory with free access to food and water, and maintained under a 12-h dark/light cycle in a room with controlled temperature (24 ± 1°C) and humidity (55 ± 5%). All procedures performed in the present study were conducted according to the guidelines approved by the Institutional Animal Care and Ethical Committee of the University of Shizuoka.

In the present *in vivo* experiments, SD/PFD was blended with lactose (43–90 μm) because the amount of drug required for *in vivo* experiments was too little to handle. The ratio of SD/PFD to lactose was 3:50 (w/w). For pharmacological experiments, RP formulation of OVA (OVA-RP) was prepared as reported previously (23). OVA particles and erythritol were first ground to fine powders with a pestle and mortar and then milled with an A-O JET MILL (Seishin Enterprise, Tokyo, Japan) at a pusher nozzle pressure and grinding nozzle pressure of 6.0 and 5.5 MPa, respectively. The ratio of OVA to erythritol was 1:400 (w/w). Micronized OVA was decompounded with a 10-fold amount of erythritol carrier particles in a plastic bag for 3 min, and the obtained dry powders of OVA were stored in a vacuum desiccator until tested.

For evaluating pharmacological efficacy, experimental lung inflammation model rats were prepared in accordance with the previous report (23) (Supplementary Fig. 1). Briefly, rats were sensitized by intraperitoneal injection of 100 μg of OVA with 5 mg aluminum hydroxide gel on days 0, 7, and 14. Then, they were anesthetized with sodium pentobarbital (50 mg/kg, i.p.) and received intratracheal administration of OVA-RP (100 μg-OVA/rat) powder at 24 h after the last OVA sensitization. At 1 h before the OVA challenge, SD/PFD (0.3 mg-PFD/rat) or lactose as control-RP was administered *via* intratracheal insufflation using a PennCentury insufflation powder delivery device (DP-4, INA Research Inc., Nagoya, Japan). A bolus (2 mL) of air from an attached

syringe was used to deliver the preloaded powder from the chamber of the insufflator into the airway of the rats. At 24 h after OVA challenge, rats were exsanguinated *via* the descending aorta under anesthesia with sodium pentobarbital, and the lungs were perfused with 30 mL of saline and removed. For pharmacokinetic analysis, rats were fasted for approximately 18 h before drug administration, and SD/PFD was administered *via* intratracheal insufflation. PFD dissolved in water containing 0.05% Tween 20 was orally administered to fasted rats (30 and 160 mg/kg).

Total Cell Counting in Bronchoalveolar Lavage Fluid

Bronchoalveolar lavage fluid (BALF) is widely used for the differential diagnosis or monitoring of lung inflammatory, and BALF cell patterns reflect inflammatory cell profiles in affected lung tissues (24). Total cell number in BALF also related to the number of inflammatory cells infiltrating in the rat lung (25); therefore, total cell counting in BALF was carried out in accordance with the previous report (14). The animals were euthanized at 24 h after OVA challenge, and BALF was immediately obtained by washing the lung *via* airways twice with 5 mL of phosphate buffered saline (PBS). Cells in BALF were isolated by centrifugation at 112 × g for 10 min. The isolated cells were re-suspended by adding 1 mL of PBS and stained by adding an equal amount of 0.2% trypan blue. The total cell number in BALF was counted using a Burker-Turk counting chamber.

Measurement of Myeloperoxidase Activity

Enzymatic detection of myeloperoxidase (MPO) in BALF was performed in accordance with a previous report (12,23). Briefly, assay mixtures consisted of 40 μL of H_2O_2 (final concentration: 0.3 mM) in 80 mM sodium phosphate buffer (pH5.4) and 50 μL of BALF sample. The reaction was initiated by addition of 10 μL of TMBZ (final concentration: 1.6 mM) in dimethyl sulfoxide at 37°C and stopped after 2 min by addition of 0.18 M H_2SO_4. Subsequently, optical density was determined at 450 nm. A titration curve of horseradish peroxidase was used for the calculation of MPO activity, which was expressed in arbitrary units. All samples were assayed in duplicate, and optical densities in all assays were measured using a SAFIRE microplate reader (TECAN, Männedorf, Switzerland).

Plasma Concentration of PFD After Intratracheal or Oral Administration

Blood samples were taken in a volume of 200 μL from the tail vein at the indicated time points (5, 15, 30, 45 min, 1, 2, 3, 4, and 6 h) after intratracheal administration of SD/PFD (0.3 mg-PFD/rat) or oral administration of PFD (30 and 160 mg/kg). The blood samples were centrifuged (10, 000 × g, 10 min, 4°C) to prepare plasma samples, which were then kept frozen at below −20°C until analyzed. Plasma samples were deproteinized by the addition of acetonitrile (plasma:acetonitrile = 2:5), mixed, and centrifuged (2000 rpm, 1 min, 4°C). The supernatants were then filtered, and 50% acetonitrile solution containing antipyrine (5 μg/mL), an internal standard, was added for UPLC/ESI-MS analysis.

UPLC Analysis

The concentrations of PFD in the plasma were determined by UPLC/ESI-MS analysis. The UPLC/ESI-MS system consisted of a Waters Acquity UPLC™ system (Waters, Milford, MA, USA), which included a binary solvent manager, a sample manager, a column compartment, and a Micromass SQ detector connected with Waters Masslynx v 4.1. A Waters Acquity UPLC™ BEH C_{18} column (particle size: 1.7 μm, column size: ϕ2.1 × 50 mm; Waters) was used, and column temperature was maintained at 40°C. The standards and samples were separated using a gradient mobile phase consisting of Milli-Q containing 5 mM ammonium acetate (A) and methanol (B). The gradient condition of the mobile phase was 0–0.5 min, 75% A; 0.5–4 min, 75–40% A; 4–5 min, 5% A; 5–6 min, 75% A, and the flow rate was set at 0.25 mL/min. Analysis was carried out using SIR for specific m/z: 186 $[M+1]^+$ for PFD; and 189 $[M+1]^+$ for antipyrine (internal standard). The present UPLC-ESI/MS protocol for the determination of PFD was validated in terms of linearity, accuracy, and precision according to the ICH guidelines "Q2B Validation of Analytical Procedures: Methodology."

Pharmacokinetic Analysis

Pharmacokinetic characterization in the plasma was performed by non-compartmental analysis as implemented in WinNonlin Professional Version 5.2 (Pharsight Corporation, Mountain View, CA, USA), and maximum concentration (C_{max}), elimination half-life ($t_{1/2}$), area under concentration *versus* time curve ($AUC_{0\text{-inf}}$), and mean residence time (MRT) were calculated based on the obtained plasma concentration-time curves.

Data Analysis

For statistical comparisons, one-way ANOVA with pairwise comparison by Fisher's least significant difference test was used. A p value of less than 0.05 was considered significant for all analyses.

RESULTS AND DISCUSSION

Physicochemical Properties of Spray-Dried Pirfenidone

Spray-drying of pharmaceuticals has been widely used as a powder manufacturing technology for producing inhalable dry powders due to its ability to modulate particle properties, including particle density, particle size, and surface morphology (26). The one-step process for preparing inhalable powders from solution, suspension, or emulsion is also an advantage of spray-drying technology. Hence, the spray-drying method was employed for preparing inhalable PFD particles. Dispersibility is also an important particle property for inhalable particles, and addition of excipients, including amino acids, lecithin, and magnesium stearate, has been used for improving dispersibility (27). In particular, L-leucine is widely used as a dispersiblity enhancer for preparing inhalable powders by spray-drying (26), and L-leucine was shown to significantly increased FPF of a formulation with high dispersibility and flowability compared with other amino acids (22). In this context, SD/PFD was prepared by spray-drying of a 30% ethanol solution containing PFD and L-leucine (9:1) in the present investigation, and the physicochemical properties of the resultant SD/PFD were assessed focusing on particle morphology, particle size, and *in vitro* inhalation performance.

The particle morphology of SD/PFD was observed by SEM, and the powders produced had corrugated surface (Fig. 1a). Addition of L-leucine resulted in spray-dried powders with dimpled surfaces, and the surface roughness of inhalable powders made a contribution to a reduction in aerodynamic diameter (22). Therefore, SD/PFD may have a favorable surface morphology for inhalation therapy. Particle size is a key particle property in defining the deposition pattern of drug particles delivered to the respiratory system using inhalers (28), and thus, the particle size distribution of the prepared SD/PFD powders was measured by laser diffraction analysis (Fig. 1b). The mean diameter and SPAN factor of the prepared SD/PFD particles were calculated to be 1.793 μm and 1.533, respectively. According to the previous report (29), inhaled powders with a diameter of around 1–5 μm are suitable for deposition in small airways and alveoli, and particles smaller than 3 μm, in particular, have a higher potential for reaching lower airways. Although particles with diameter of less than 0.5 μm can be inhaled into the deep lung, these particles are likely to be exhaled before deposition. Thus, the prepared SD/PFD powders have an optimal size distribution for pulmonary delivery, and inhalation of SD/PFD may have a high therapeutic potential for IPF. For further characterization, the *in vitro* inhalation performance of SD/PFD was examined using the NGI system with Osmohaler™ (Fig. 1c). From the deposition profile obtained from the NGI analysis, the emitted dose and FPF value of SD/PFD were calculated to be 73.3 and 62.4%, respectively.

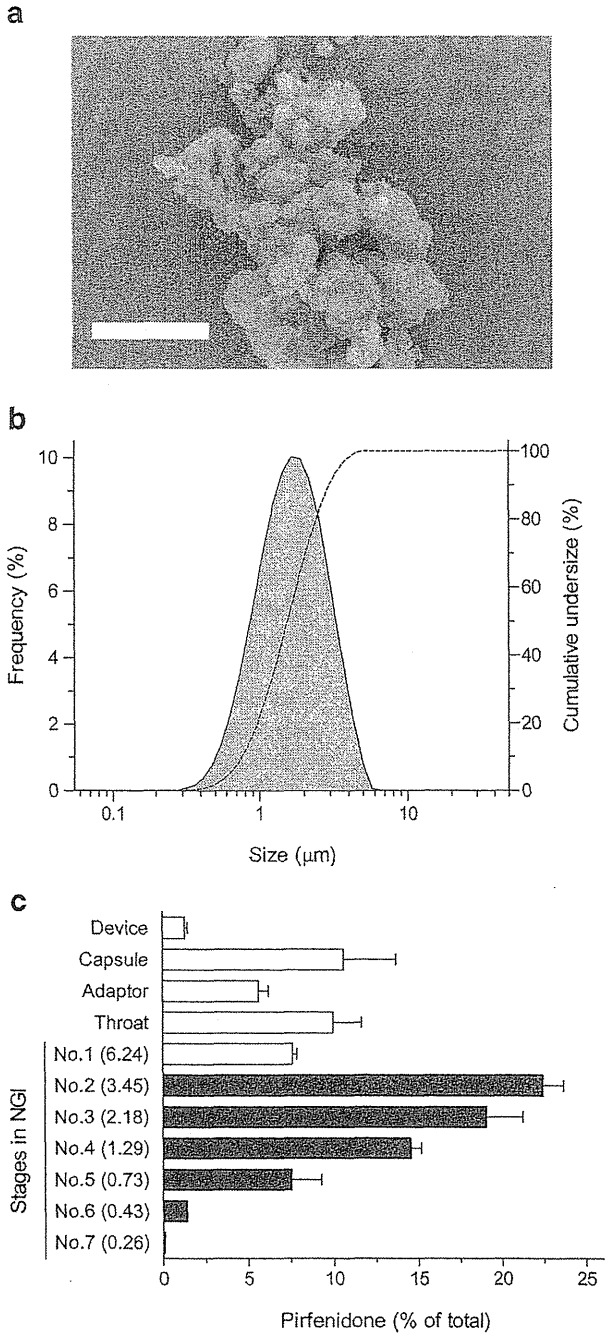

Fig. 1 *In vitro* particle characterization of SD/PFD. (**a**) A scanning electron microscopic image of SD/PFD. *Bar* represents 5 μm. (**b**) Particle size distribution of SD/PFD as determined by laser diffraction particle size analysis. *Solid line*, frequency; and *dotted line*, cumulative undersize fraction curve. (**c**) Deposition pattern of SD/PFD powders in the NGI. Data represent mean ± SD for three experiments. The *number in parenthesis* represents a cutoff diameter (μm) for each stage.

Interestingly, SD/PFD particles achieved a high FPF value without the need of carrier particles. In the previous investigation, PFD-RP was prepared with lactose carriers, and the FPF value of PFD-RP obtained from cascade impactor

analysis was found to be 23.4% (14); therefore, SD/PFD would allow more efficient pulmonary delivery compared with PFD-RP by comparison of the FPF values, and SD/PFD may be made available as a carrier-free inhalable powder formulation for the treatment of IPF. In the development of RP systems, carrier particles, such as lactose and other sugars, are usually blended for improving the flowability and dispersibility of drug microparticles and nanoparticles (30); however, the drug loading amount is limited in carrier-blended RP systems because of the presence of excessive carrier particles (31,32). On the other hand, SD/PFD would achieve high drug loading amount due to the lack of carrier particle requirement for inhalation, possibly leading to better clinical outcomes.

Anti-Inflammatory Effects in an Experimental Airway Inflammation Model

To clarify the therapeutic potential of SD/PFD, the anti-inflammatory effects of insufflated SD/PFD were evaluated in an antigen-evoked lung inflammation model (23). SD/PFD was intratracheally administered at 1 h before OVA-RP challenge, followed by collection of BALF for counting the number of inflammatory cells at 24 h after OVA-RP insufflation (Fig. 2a). SD/PFD at a dose of 0.3 mg-PFD/rat was employed for intratracheal administration because insufflated PFD-RP at 0.3 mg-PFD/rat or higher was reported to attenuate inflammatory events in the airway system (14). After intratracheal administration of OVA-RP, significant recruitment of inflammatory cells in BALF was observed as evidenced by approximately 4.8-fold increase of total cell number, mainly consisting of monocytes and neutrophils. On the other hand, recruitment of inflammatory cells in BALF in response to insufflated OVA-RP was significantly attenuated by pre-insufflation of SD/PFD (0.3 mg-PFD/rat) with approximately 83% reduction of infiltrated cells, and no significant differences were observed between non-sensitized and OVA-sensitized rats pretreated with SD/PFD. These results suggested that insufflated SD/PFD may have a therapeutic potential for airway inflammation.

In the OVA-evoked airway inflammation model, infiltration of neutrophils was observed as one of the main infiltrating inflammatory cells after OVA-RP challenge, consistent with the previous report (23). MPO is a pro-inflammatory and pro-oxidant enzyme, mainly released from activated neutrophils and macrophages (33); therefore, for further characterization of the anti-inflammatory effects of SD/PFD in the antigen-evoked asthma/COPD model, MPO activity in BALF was also investigated (Fig. 2b). OVA-RP challenge caused an approximate 2.5-fold elevation of MPO level in BALF, suggesting the development of pulmonary neutrophilia in OVA-sensitized rats. Pretreatment of SD/PFD tended to suppress the up-regulation of MPO activity in BALF caused by OVA-

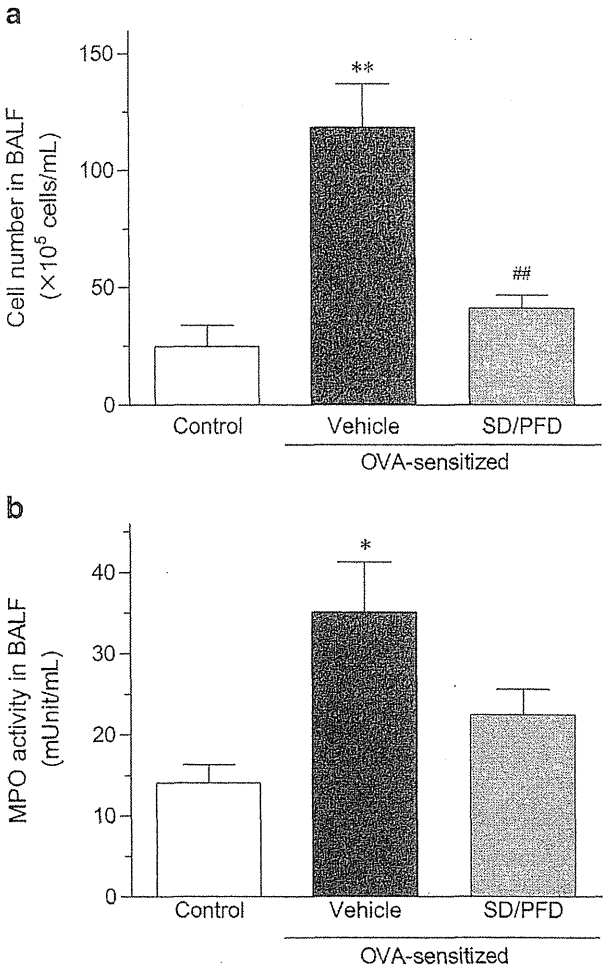

Fig. 2 Anti-inflammatory effects of insufflated SD/PFD in OVA-evoked airway inflammation model. At 24 h after the OVA challenge, (**a**) recruited inflammatory cells and (**b**) MPO activity in BALF were monitored with or without pre-insufflation of SD/PFD (0.3 mg-PFD/rat). Data represent mean ± SE for six experiments. *, $P < 0.05$ and **, $P < 0.01$ with respect to non-sensitized rats with insufflation of control-RP. ##, $P < 0.01$ with respect to OVA-sensitized rats with insufflation of control-RP.

RP challenge, possibly indicating its potential for treatment of neutrophilia in the airway system. In the previous reports, an increase of neutrophils in bronchoalveolar lavage was observed in 70–90% of IPF patients (34), and neutrophilic inflammation was reported to be a pathogenic factor of IPF (35). Therefore, the use of an antigen-evoked asthma/COPD model would be adequate for evaluating the pharmacological efficacy of insufflated SD/PFD, and the present results suggest the topical therapeutic potential of SD/PFD against pulmonary inflammation in the early stages of IPF.

In the previous report, anti-inflammatory effects of orally-administered PFD at 30 mg/kg were confirmed in experimental models, including antigen-induced and LPS-induced acute inflammation models (36). On the other hand, a high anti-inflammatory effect was observed after pre-insufflation of

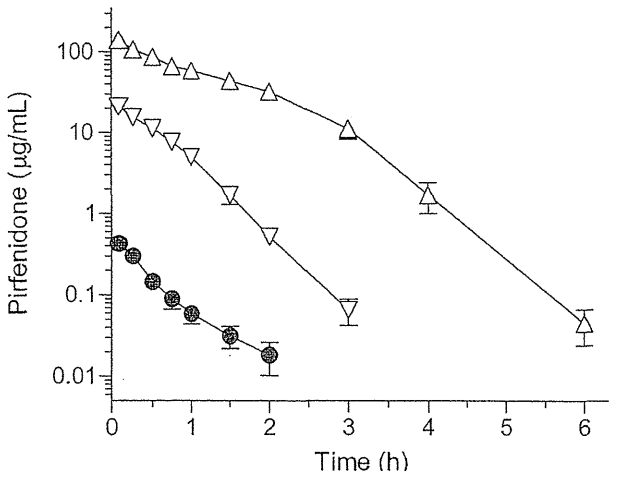

Fig. 3 Plasma concentration-time profiles of PFD after intratracheal administration of SD/PFD and oral administration of PFD in rats. ●, insufflated SD/PFD at a pharmacologically effective dose (0.3 mg-PFD/rat); △, orally-administered PFD at a phototoxic dose (160 mg/kg); and ▽, orally-administered PFD at a non-phototoxic dose (30 mg/kg). Each value represents mean ± SE for five rats.

SD/PFD at 0.3 mg-PFD/rat (approximately 1 mg-PFD/kg) in the present study, suggesting that SD/PFD may be effective at lower doses compared with orally-administered PFD. Although this comparison may not be appropriate due to the different experimental conditions, SD/PFD may achieve marked reductions in the pharmacologically effective dose of PFD for lung disease. Regarding treatment of pulmonary fibrosis, the pharmacologically effective dose of RP systems of PFD for treating pulmonary fibrosis is still unclear. In the previous investigation, fibrocyte accumulation in the lung was attenuated after oral administration of PFD at 300 mg/kg/day for 2 weeks in a bleomycin-induced pulmonary fibrosis model (37). Thus, the appropriate dosage of RP formulations of PFD for treatment of pulmonary fibrosis should be further investigated in pulmonary fibrosis models.

Pharmacokinetic Analysis of Pirfenidone After Oral or Intratracheal Administration

According to the *in vivo* pharmacological experiments, insufflated SD/PFD (0.3 mg-PFD/rat) achieved favorable anti-inflammatory outcomes in an antigen-evoked airway inflammation model; however, systemic exposure risk after insufflation of SD/PFD is still unclear. Hence, a pharmacokinetic study of PFD was conducted after intratracheal administration of SD/PFD at a pharmacologically effective dose (0.3 mg-PFD/rat) to investigate systemic exposure risk. In general, particle size reduction results in high membrane permeability and improved bioavailability (38). Additionally, permeability in the lung is higher than that in the intestine because the lung has a large surface area attributed to numerous alveoli and the thin layer of alveolar cells (39,40). The RP formulations of PFD was developed for reducing systemic exposure of PFD compared with oral administration of PFD, possibly leading to low toxicity risk (14); therefore, to investigate the toxicity risk of SD/PFD, a comparative pharmacokinetic study of PFD in rats was also performed after oral administration of PFD at non-phototoxic and phototoxic doses (30 and 160 mg/kg, respectively) (10). Plasma concentration-time curves of PFD were obtained by UPLC/ESI-MS analysis of samples taken after intratracheal and oral administration of PFD formulations (Fig. 3). The pharmacokinetic parameters of PFD were calculated on the basis of the plasma concentration-time profiles obtained (Table I). After intratracheal administration of SD/PFD (0.3 mg-PFD/rat), the plasma concentration reached C_{max} within 5 min, as did orally-administered PFD (30 and 160 mg/kg). Plasma concentrations then rapidly decreased with a $t_{1/2}$ of approximately 0.3–0.5 h. According to the calculated C_{max} and AUC_{0-inf} in the plasma, the systemic exposure level of PFD after insufflation of SD/PFD at the pharmacologically effective dose was much lower than those after oral administration of PFD at both non-phototoxic and phototoxic doses. Compared with orally-administered PFD at the phototoxic dose, insufflated SD/PFD at the pharmacologically effective dose led to approximately 280- and 600-fold reductions in C_{max} and AUC_{0-inf} values, respectively. In addition, 42- and 52-fold differences in C_{max} and AUC_{0-inf} values, respectively, were still observed between insufflated SD/PFD at the pharmacologically effective dose and oral administration of PFD at the non-phototoxic dose. On the other hand, there were no differences in the duration of systemic exposure of PFD among the intratracheal and oral administrations of PFD formulations on the basis of the $t_{1/2}$ and MRT values. From these findings, compared with oral therapy of PFD for IPF, inhalation therapy with the use of

Table I Pharmacokinetic Parameters of PFD After Intratracheal and Oral Administrations

	C_{max} (μg/mL)	$t_{1/2}$ (h)	AUC_{0-inf} (h · μg/mL)	MRT (h)
SD/PFD (0.3 mg-PFD/rat, i.t.)	0.499 ± 0.086	0.32 ± 0.04	0.266 ± 0.051	0.583 ± 0.060
PFD (30 mg/kg, p.o.)	21.0 ± 1.4	0.33 ± 0.02	13.7 ± 0.94	0.576 ± 0.028
PFD (160 mg/kg, p.o.)	139 ± 11	0.53 ± 0.03	159 ± 10	1.10 ± 0.075

Each parameter was calculated on the basis of the plasm concentration-time curves. Each value represents mean ± S.E. for five rats

SD/PFD would attenuate systemic exposure risk with improved photosafety of PFD.

In the previous investigation, insufflated PFD-RP at the pharmacologically effective dose indicated low systemic exposure levels, and deposition to UV-exposed tissues was reduced after insufflation of PFD-RP compared with orally-administered PFD at both non-phototoxic and phototoxic doses. Therefore, insufflated SD/PFD may similarly modurate deposition of PFD in light-exposed tissues due to its low systemic exposure. Furthermore, the limited systemic exposure after insufflation of RP formulations of PFD may attenuate other adverse effects induced by orally-administered PFD, including hepatic dysfunction and gastrointestinal discomfort. Thus, further investigations of RP formulation of PFD focusing on hepatotoxicity and gastrointestinal tract disturbance are warranted. Inhalation therapy with the use of RP systems for PFD would be an attractive alternative to current oral therapy of PFD for treating IPF.

CONCLUSION

A new RP system of PFD with favorable inhalation properties and lowered systemic exposure risk was developed using the spray-drying method. Prepared SD/PFD powder had favorable surface morphology and particle size distribution for inhalation, and the high *in vitro* inhalation performance of SD/PFD was observed without the need of carrier particles in NGI analysis. In the antigen-evoked airway inflammation model, insufflated SD/PFD attenuated inflammatory events in the lung after OVA-RP challenge. Regarding the pharmacokinetic behaviors, insufflation of SD/PFD at the pharmacologically effective dose reduced systemic exposure levels of PFD compared with orally-administered PFD at both non-phototoxic and phototoxic dose, suggesting a lowered risk of systemic side effects. From these findings, the RP system with the use of SD/PFD would allow effective treatment of IPF with a wide safety margin.

ACKNOWLEDGMENTS AND DISCLOSURES

This work was supported by Grant-in-Aid for Young Scientists (B) from the Ministry of Education, Science, Sports and Culture, Japan. Sharon Shui Yee Leung was supported by Faculty of Pharmacy postdoctoral fellowship at the University of Sydney.

REFERENCES

1. Schaefer CJ, Ruhrmund DW, Pan L, Seiwert SD, Kossen K. Antifibrotic activities of pirfenidone in animal models. Eur Respir Rev. 2011;20:85–97.
2. Iyer SN, Gurujeyalakshmi G, Giri SN. Effects of pirfenidone on transforming growth factor-beta gene expression at the transcriptional level in bleomycin hamster model of lung fibrosis. J Pharmacol Exp Ther. 1999;291:367–73.
3. Hisatomi K, Mukae H, Sakamoto N, Ishimatsu Y, Kakugawa T, Hara S, *et al.* Pirfenidone inhibits TGF-beta1-induced overexpression of collagen type I and heat shock protein 47 in A549 cells. BMC Pulm Med. 2012;12:24.
4. Lasky J. Pirfenidone. IDrugs. 2004;7:166–72.
5. Takeda Y, Tsujino K, Kijima T, Kumanogoh A. Efficacy and safety of pirfenidone for idiopathic pulmonary fibrosis. Patient Prefer Adher. 2014;8:361–70.
6. Hilberg O, Simonsen U, du Bois R, Bendstrup E. Pirfenidone: significant treatment effects in idiopathic pulmonary fibrosis. Clin Respir J. 2012;6:131–43.
7. Richeldi L, Yasothan U, Kirkpatrick P. Pirfenidone. Nat Rev Drug Discov. 2011;10:489–90.
8. Taniguchi H, Ebina M, Kondoh Y, Ogura T, Azuma A, Suga M, *et al.* Pirfenidone in idiopathic pulmonary fibrosis. Eur Respir J. 2010;35:821–9.
9. Carter NJ. Pirfenidone: in idiopathic pulmonary fibrosis. Drugs. 2011;71:1721–32.
10. Seto Y, Inoue R, Kato M, Yamada S, Onoue S. Photosafety assessments on pirfenidone: photochemical, photobiological, and pharmacokinetic characterization. J Photochem Photobiol B. 2013;120:44–51.
11. International Council on Harmonisation of Technical Requirements for Registration of Pharmaceuticals for Human Use (ICH). ICH Guideline S10 Guidance on photosafety evaluation of pharmaceuticals. 2013.
12. Onoue S, Aoki Y, Kawabata Y, Matsui T, Yamamoto K, Sato H, *et al.* Development of inhalable nanocrystalline solid dispersion of tranilast for airway inflammatory diseases. J Pharm Sci. 2011;100:622–33.
13. Onoue S, Sato H, Kawabata Y, Mizumoto T, Hashimoto N, Yamada S. In vitro and in vivo characterization on amorphous solid dispersion of cyclosporine A for inhalation therapy. J Control Release. 2009;138:16–23.
14. Onoue S, Seto Y, Kato M, Aoki Y, Kojo Y, Yamada S. Inhalable powder formulation of pirfenidone with reduced phototoxic risk for treatment of pulmonary fibrosis. Pharm Res. 2013;30:1586–96.
15. Buttini F, Colombo P, Rossi A, Sonvico F, Colombo G. Particles and powders: tools of innovation for non-invasive drug administration. J Control Release. 2012;161:693–702.
16. Lin YW, Wong J, Qu L, Chan HK, Zhou QT. Powder production and particle engineering for dry powder inhaler formulations. Curr Pharm Des. 2015;21:3902–16.
17. Belotti S, Rossi A, Colombo P, Bettini R, Rekkas D, Politis S, *et al.* Spray-dried amikacin sulphate powder for inhalation in cystic fibrosis patients: the role of ethanol in particle formation. Eur J Pharm Biopharm. 2015;93:165–72.
18. Lee SH, Teo J, Heng D, Zhao Y, Ng WK, Chan HK, *et al.* A novel inhaled multi-pronged attack against respiratory bacteria. Eur J Pharm Sci. 2015;70:37–44.
19. Zhou QT, Morton DA, Yu HH, Jacob J, Wang J, Li J, *et al.* Colistin powders with high aerosolisation efficiency for respiratory infection: preparation and in vitro evaluation. J Pharm Sci. 2013;102:3736–47.
20. Aquino RP, Stigliani M, Del Gaudio P, Mencherini T, Sansone F, Russo P. Nanospray drying as a novel technique for the manufacturing of inhalable NSAID powders. Scientific World J. 2014;2014:838410.
21. Onoue S, Sato H, Ogawa K, Kojo Y, Aoki Y, Kawabata Y, *et al.* Inhalable dry-emulsion formulation of cyclosporine A with improved anti-inflammatory effects in experimental asthma/COPD-model rats. Eur J Pharm Biopharm. 2012;80:54–60.

22. Chew NY, Shekunov BY, Tong HH, Chow AH, Savage C, Wu J, *et al.* Effect of amino acids on the dispersion of disodium cromoglycate powders. J Pharm Sci. 2005;94:2289–300.
23. Misaka S, Sato H, Yamauchi Y, Onoue S, Yamada S. Novel dry powder formulation of ovalbumin for development of COPD-like animal model: physicochemical characterization and biomarker profiling in rats. Eur J Pharm Sci. 2009;37:469–76.
24. Costabel U, Guzman J. Bronchoalveolar lavage in interstitial lung disease. Curr Opin Pulm Med. 2001;7:255–61.
25. Misaka S, Aoki Y, Karaki S, Kuwahara A, Mizumoto T, Onoue S, *et al.* Inhalable powder formulation of a stabilized vasoactive intestinal peptide (VIP) derivative: anti-inflammatory effect in experimental asthmatic rats. Peptides. 2010;31:72–8.
26. Vehring R. Pharmaceutical particle engineering via spray drying. Pharm Res. 2008;25:999–1022.
27. Begat R, Price R, Harris H, Morton DAV, Staniforth JN. The influence of force control agents on the cohesive-adhesive balance in dry powder inhaler formulations. KONA. 2005;23:109–21.
28. Suarez S, Hickey AJ. Drug properties affecting aerosol behavior. Respir Care. 2000;45:652–66.
29. Labiris NR, Dolovich MB. Pulmonary drug delivery. part I: physiological factors affecting therapeutic effectiveness of aerosolized medications. Br J Clin Pharmacol. 2003;56:588–99.
30. Pilcer G, Amighi K. Formulation strategy and use of excipients in pulmonary drug delivery. Int J Pharm. 2010;392:1–19.
31. Healy AM, Amaro MI, Paluch KJ, Tajber L. Dry powders for oral inhalation free of lactose carrier particles. Adv Drug Deliv Rev. 2014;75:32–52.
32. Zhou QT, Leung SS, Tang P, Parumasivam T, Loh ZH, Chan HK. Inhaled formulations and pulmonary drug delivery systems for respiratory infections. Adv Drug Deliv Rev. 2015;85:83–99.
33. Winterbourn CC, Vissers MC, Kettle AJ. Myeloperoxidase. Curr Opin Hematol. 2000;7:53–8.
34. Pesci A, Ricchiuti E, Ruggiero R, De Micheli A. Bronchoalveolar lavage in idiopathic pulmonary fibrosis: what does it tell us? Respir Med. 2010;104 Suppl 1:S70–73.
35. Beeh KM, Beier J, Kornmann O, Buhl R. Neutrophilic inflammation in induced sputum of patients with idiopathic pulmonary fibrosis. Sarcoidosis Vasc Diffuse Lung Dis. 2003;20:138–43.
36. Spond J, Case N, Chapman RW, Crawley Y, Egan RW, Fine J, *et al.* Inhibition of experimental acute pulmonary inflammation by pirfenidone. Pulm Pharmacol Ther. 2003;16:207–14.
37. Inomata M, Kamio K, Azuma A, Matsuda K, Kokuho N, Miura Y, *et al.* Pirfenidone inhibits fibrocyte accumulation in the lungs in bleomycin-induced murine pulmonary fibrosis. Respir Res. 2014;15:16.
38. Onoue S, Yamada S, Chan HK. Nanodrugs: pharmacokinetics and safety. Int J Nanomed. 2014;9:1025–37.
39. Patton JS, Fishburn CS, Weers JG. The lungs as a portal of entry for systemic drug delivery. Proc Am Thorac Soc. 2004;1:338–44.
40. Patton JS, Byron PR. Inhaling medicines: delivering drugs to the body through the lungs. Nat Rev Drug Discov. 2007;6:67–74.

Regulatory Toxicology and Pharmacology 72 (2015) 578–585

Contents lists available at ScienceDirect

Regulatory Toxicology and Pharmacology

journal homepage: www.elsevier.com/locate/yrtph

Non-animal photosafety screening for complex cosmetic ingredients with photochemical and photobiochemical assessment tools

Hayato Nishida [a], Morihiko Hirota [a], Yoshiki Seto [b], Gen Suzuki [b], Masashi Kato [b], Masato Kitagaki [a], Mariko Sugiyama [a], Hirokazu Kouzuki [a], Satomi Onoue [b,*]

[a] Shiseido Research Center, Shiseido Co. Ltd., 2-2-1 Hayabuchi, Tsuzuki-ku, Yokohama-shi, Kanagawa 224-8558, Japan
[b] Department of Pharmacokinetics and Pharmacodynamics, School of Pharmaceutical Sciences, University of Shizuoka, 52-1 Yada, Suruga-ku, Shizuoka 422-8526, Japan

ARTICLE INFO

Article history:
Received 24 February 2015
Available online 3 June 2015

Keywords:
Cosmetics
Complex cosmetic ingredients
Photosafety assessment
Phototoxicity
Reactive oxygen species

ABSTRACT

Previously, a non-animal screening approach was proposed for evaluating photosafety of cosmetic ingredients by means of *in vitro* photochemical and photobiochemical assays; however, complex cosmetic ingredients, such as plant extracts and polymers, could not be evaluated because their molecular weight is often poorly defined and so their molar concentration cannot be calculated. The aim of the present investigation was to establish a photosafety screen for complex cosmetic ingredients by using appropriately modified *in vitro* photosafety assays. Twenty plant extracts were selected as model materials on the basis of photosafety information, and their phototoxic potentials were assessed by means of ultraviolet (UV)/visible light (VIS) spectral analysis, reactive oxygen species (ROS)/micellar ROS (mROS) assays, and 3T3 neutral red uptake phototoxicity testing (3T3 NRU PT). The maximum UV/VIS absorption value was employed as a judgment factor for evaluating photoexcitability of samples, and the value of 1.0 was adopted as a tentative criterion for photosafety identification. The ROS/mROS assays were conducted at 50 μg/mL, and no false negative prediction was obtained. Furthermore, the ROS/mROS assays at 50 μg/mL had a similar predictive capacity to the ROS/mROS assays in the previous study. A systematic tiered approach for simple and rapid non-animal photosafety evaluation of complex cosmetic ingredients can be constructed using these modified *in vitro* photochemical assays.

1. Introduction

Cosmetics applied to the skin are likely to be directly exposed to sunlight containing ultraviolet (UV) and visible light (VIS) (290–700 nm), and some cosmetic ingredients are known to induce phototoxic skin responses (Moore, 2002); therefore, the photosafety of ingredients is one of the major concerns in safety assessments during product development. Phototoxic skin responses can be divided at least three types: photoirritation, photoallergy, and photogenotoxicity (Epistein, 1983; Onoue and Tsuda, 2006). Among them phototoxicity (photoirritation) and photoallergy are the main targets of photosafety assessments according to the International Conference on Harmonisation of Technical Requirements for Registration of Pharmaceuticals for Human Use (ICH) S10 guideline (ICH, 2014). For evaluating the risk of phototoxic skin reactions, *in vivo* phototoxicity and photoallergy tests employing guinea pigs, rabbits, rats, and mice used to be carried out; however, following the implementation of the 3Rs principle (refinement, reduction, replacement), *in vivo* photosafety tests are not currently undertaken in the cosmetic industry. The 7th Amendment (Directive 2003/15/EC) to the Cosmetic Directive (Directive76/768/EEC) called for a marketing ban from March 2013 on cosmetic products containing ingredients that have been tested in animals for toxicity, and therefore, various *in vitro* photosafety assessment tools have been developed as alternatives to *in vivo* experiments (Seto et al., 2012). However, a reliable and comprehensive non-animal photosafety screening strategy is still urgently needed.

Abbreviations: 3T3 NRU PT, 3T3 neutral red uptake phototoxicity testing; DMSO, dimethyl sulfoxide; EBSS, Earle's balanced salt solution; ECVAM, European Centre for Validation of Alternative Methods; ICH, International Conference on Harmonization of Technical Requirements for Registration of Pharmaceuticals for Human Use; IFRA, International Fragrance Association; MEC, molar extinction coefficient; mROS assay, micellar ROS assay; NaPB, sodium phosphate buffer; NBT, nitroblue tetrazolium; OECD, Organisation for Economic Co-operation and Development; photo-h-CLAT, photo human cell line activation test; PIF, photoirritation factor; ROS, reactive oxygen species; SCCS, Scientific Committee on Consumer Safety; UV, ultraviolet; VIS, visible light.

* Corresponding author. Fax: +81 54 264 5636.
E-mail address: onoue@u-shizuoka-ken.ac.jp (S. Onoue).

http://dx.doi.org/10.1016/j.yrtph.2015.05.029
0273-2300/

Guidance on the photosafety testing of medicinal products was established by regulatory agencies in the US and EU in the early 2000s (Seto et al., 2012). In addition, the recent ICH S10 photosafety guideline has provided a detailed framework and guidance for photosafety evaluation in the pharmaceutical industry (ICH, 2014). These guidelines propose photosafety assessment strategies based on photochemical and photobiochemical properties, and *in vivo* pharmacokinetic behaviors (EMEA/CPMP, 2002; FDA/CDER, 2002; OECD, 2004; ICH, 2014). In the previous study, the strategic use of the *in vitro* photochemical and photobiochemical methods described in the ICH S10 guideline might enable reliable photosafety prediction for cosmetics ingredients (Onoue et al., 2013a). Thirty-four phototoxic chemicals including 20 cosmetic ingredients and 14 non-cosmetics were correctly detected as positives using *in vitro* photochemical methods such as a UV/VIS spectral analysis (Henry et al., 2009), reactive oxygen species (ROS) assay (Onoue et al., 2013a), and micellar ROS (mROS) assay for lipophilic chemicals (Seto et al., 2013). However, molar concentration is generally employed as a unit of chemical concentration for calculating molar extinction coefficient (MEC) in UV/VIS spectral analysis and for photoreactivity evaluation in the ROS/mROS assays. In the cosmetics industry, complex cosmetic ingredients, including plant extracts and polymers, are widely used, and *in vitro* photochemical methodologies using molar concentration are not applicable to complex cosmetic ingredients having poorly defined molecular weights. Thus, modification of the existing *in vitro* methods is necessary to make them applicable for photosafety prediction of complex cosmetic ingredients.

The major purpose of this study is to establish a photosafety prediction strategy for complex cosmetic ingredients with undefined molecular weight, employing *in vitro* photochemical and photobiochemical data. In this study, 11 phototoxic and 9 non-phototoxic plant extracts were used as model substances, and identified suitable conditions for evaluating their photochemical and photobiochemical properties with the use of UV/VIS spectral analysis, ROS/mROS assays, and 3T3 neutral red uptake phototoxicity testing (3T3 NRU PT). The UV/VIS spectral analysis was carried out for 7 phototoxic plant extracts at their limit concentrations as described in the International Fragrance Association (IFRA) standards booklet (IFRA, 2013), and the maximum UV/VIS absorption value was employed as an alternative to MEC value. In the ROS/mROS assays, ROS generation from 20 irradiated plant extracts at the concentration of 50 μg/mL was monitored, and the photoreactivity of tested samples was judged on the basis of the criteria for the validated ROS assay. 3T3 NRU PT was also applied to the 20 plant extracts. Finally, a photosafety screening strategy was proposed on the basis of the obtained photochemical and photobiochemical data.

2. Materials and methods

2.1. Materials

2.1.1. Plant materials

Twenty plant materials including 11 phototoxic and/or photoallergic substances were used. Eight plant extracts were employed as model phototoxic substances referring to the globally accepted IFRA standards (IFRA, 2013), and 3 other plant materials were also selected on the basis of reported information (Onoue et al., 2009). Nine plant extracts were defined as non-phototoxic materials according to the following criteria: (i) widely used as foods and cosmetic ingredients for human use; and (ii) no reports of phototoxic skin reactions. Angelica root oil (**1**), bergamot oil (**2**), celery seed oil (**3**), cumin seed oil (**4**), lemon oil (**6**), lime oil (**7**), tagetes oil (**10**), verbena oil (**11**), carrot oil (**41**), ginger oil (**43**), and lemongrass oil (**44**) were obtained from Sigma-Aldrich Japan (Tokyo, Japan). Grapefruit oil (**5**), corn oil (**42**), olive oil (**45**), rapeseed oil (**47**), safflower oil (**48**), and soybean oil (**49**) were purchased from Wako Pure Chemical Industries (Osaka, Japan). Oil parsley (**8**), St. John's wort powder (**9**), and orange oil (**46**) were obtained from Nacarai Tesque (Kyoto, Japan).

2.1.2. Chemicals and reagents

To clarify the predictive capacity of the ROS/mROS assays, 46 chemicals were selected as model chemicals on the basis of the previous study (Onoue et al., 2013a). Dimethyl sulfoxide (DMSO, **63**), *p*-nitrosodimethylaniline, imidazole, nitroblue tetrazolium (NBT), Tween 20, 4-methyl-7-ethoxycoumarin (**12**), 7-methoxycoumarin (**15**), 8-methoxypsoralen (**16**), hexachlorophene (**21**), methyl β-naphthylketone (**22**), *p*-phenylenediamine (**27**), acridine (**29**), amiodarone HCl (**30**), chlorpromazine HCl (**31**), diclofenac Na (**32**), fenofibrate (**34**), indomethacin (**35**), ketoprofen (**36**), piroxicam (**37**), promethazine HCl (**38**), quinine HCl·2H_2O, sulfanilamide (**39**), tetracycline HCl (**40**), 1,3-butylene glycol (**50**), 2-propanol (**51**), 4′-methylbenzylidene camphor (**52**), ethanol (**55**), glycerine (**56**), and isopropyl myristate (**57**) were obtained from Wako Pure Chemical Industries. Bithionol (**18**), dichlorophene (**19**), musk ketone (**25**), triclocarban (**28**), enoxacin (**33**), sulisobenzone (**62**), lactic acid (**64**), and penicillin G (**66**) were purchased from Sigma-Aldrich Japan. Benzophenone (**17**), lauric acid (**58**), propylene glycol (**59**), sodium lauryl sulfate (**61**), and methylsalicylate (**65**) were obtained from Junsei Chemical Co. (Tokyo, Japan), and 5-methoxypsoralen (**13**), 6-methylcoumarin (**14**), ascorbic acid (**53**), cetyl alcohol (**54**), and sodium laurate (**60**) were purchased from Nacalai Tesque. Fenticlor (**20**), methyl-*N*-methylanthranilate (**23**), musk ambrette (**24**), and musk xylene (**26**) were purchased from Tokyo Chemical Industry (Tokyo, Japan).

2.2. UV/VIS spectral analysis

Each plant extract was dissolved in ethanol. UV/VIS absorption spectra (290–700 nm) were measured using a UV–VIS Multipurpose Spectrophotometer MPS-2400 (Shimadzu Corporation, Kyoto, Japan) interfaced to a PC for data processing (software; UV Probe Version 1.12). A spectrofluorimeter quartz cell with 10 mm pathlength was employed.

2.3. ROS/mROS assays

2.3.1. Irradiation conditions

The ROS and mROS assays were conducted using an Atlas Suntest CPS plus (Atlas Material Technology LLC, Chicago, IL, USA) equipped with a xenon arc lamp (1500 W) and a cooling unit SR-P20FLE (Hitachi, Tokyo, Japan). A UV special filter was installed to adapt the spectrum of the artificial light source to that of natural daylight; the Atlas Suntest CPS series has a high irradiance capability that meets CIE85/1989 daylight simulation requirements. The irradiation test was carried out at 25 °C with an irradiance of ca. 2.0 mW/cm^2 as determined with a calibrated UVA detector Dr. Hönle#0037 (Dr. Hönle, München, Germany).

2.3.2. Assay procedures

The ROS assay was carried out as reported, with minor modifications (Onoue et al., 2013b). Briefly, all tested substances were dissolved in DMSO at 2.5 mg/mL to prepare stock solutions. Singlet oxygen generated from samples in 20 mM sodium phosphate buffer (NaPB; pH 7.4) after irradiation with light was measured by monitoring the bleaching of *p*-nitrosodimethylaniline at 440 nm in the presence of imidazole as a selective acceptor of singlet oxygen. Test substances (50 μg/mL), *p*-nitrosodimethylaniline

(50 μM) and imidazole (50 μM) in 20 mM NaPB were mixed in a tube. Aliquots of 200 μL of the samples were transferred into wells of a plastic 96-well plate (Asahi Glass Co., Ltd., Tokyo, Japan; code number 3881-096; clear, untreated, flat-bottomed) in triplicate and checked for precipitation before light exposure. The absorbance at 440 nm of each well was measured with a SAFIRE unit (TECAN, Männedorf, Switzerland). The plate was fixed in a quartz reaction container with a quartz cover (Ozawa Science, Aichi, Japan), and then irradiated with simulated sunlight for 1 h. After agitation on a plate shaker, the absorbance at 440 nm was measured. For the determination of superoxide anion, reduction of NBT by irradiated test substances was monitored in terms of increase of absorbance at 560 nm. Test substances (50 μg/mL) and NBT (50 μM) in 20 mM NaPB were mixed in a tube, and the absorbance at 560 nm was measured in the same manner as described for the singlet oxygen determination. To avoid false predictions due to spectral interference at 440 nm for singlet oxygen determination and at 560 nm for detection of superoxide generation, experimental controls in which test substances alone were exposed to simulated sunlight were conducted, and the control values were subtracted from sample values.

The mROS assay was conducted as reported with minor modifications (Seto et al., 2013), since some samples could not be tested in the standard assay due to limited aqueous solubility. The assay procedure was almost the same as that of the ROS assay, except that a micellar solution of 0.5% Tween 20 was added to the assay mixtures and experimental controls (test substances alone) for measuring singlet oxygen and superoxide generation.

2.3.3. Criteria for data acceptance and judgment in the ROS and mROS assays

Photoreactivity of samples (50 μg/mL) was evaluated according to the criteria used in the previous report (Onoue et al., 2008). The photoreactivity of each tested substance should be judged as follows, based on the mean value of triplicate determinations in ROS or mROS assay: (i) positive for singlet oxygen ($\Delta A_{440nm} \times 10^3$): 25 or more; and/or superoxide ($\Delta A_{560nm} \times 10^3$): 20 or more, or (ii) negative for singlet oxygen ($\Delta A_{440nm} \times 10^3$): less than 25, and superoxide ($\Delta A_{560nm} \times 10^3$): less than 20. The final determination should be made as follows: (i) positive: above the threshold level for either singlet oxygen or superoxide; or (ii) negative: below the threshold level for both singlet oxygen and superoxide.

2.3.4. 3T3 NRU PT

In vitro 3T3 NRU PT was carried out as described in the OECD 432 guideline with minor modifications (OECD, 2004). Briefly, Balb/c 3T3 cells were maintained in culture for 24 h for formation of monolayers. Two 96-well plates per plant extract were then pre-incubated with six different concentrations of the plant extract dissolved in Earle's balanced salt solution (EBSS) for 1 h in duplicate. One plate was exposed to a dose of 5 J/cm^2 UVA (+Irr experiment), and the other plate was kept in the dark by covering it with aluminum foil (−Irr experiment). UVA irradiation was performed using a sol 500 Sun simulator (Dr. Hönle) equipped with a 500 W metal halide lamp and a H-1 filter to remove potentially cytotoxic UVB wavelengths. The treatment medium was then replaced with culture medium and after 24 h, the cell viability was determined in terms of neutral red uptake for 3 h. After that, cells were lysed in ethanol:water:acetic acid = 50:49:1, and the neutral red uptake was measured as absorbance at 540 nm using a Benchmark™ Plus microplate spectrophotometer (BioRad, Hercules, CA, USA). Cell viability obtained at each of the six concentrations of the plant extract was compared with that of untreated controls, and the percent inhibition was calculated. For prediction of phototoxic potential, the concentration responses obtained in the presence and in the absence of UVA irradiation were compared, usually at the IC_{50} level, i.e. the concentration inhibiting cell viability by 50% compared to untreated controls. The photo-irritancy factor (PIF) was calculated according to the following equation:

$$PIF = \frac{IC_{50}(-Irr)}{IC_{50}(+Irr)}.$$

3. Results and discussion

3.1. UV/VIS spectral analysis

The initial step of phototoxic reactions is excitation of photoreactive substances by absorption of a photon from sunlight. To evaluate the UV/VIS absorption capacity of substances, UV/VIS spectral analysis is usually conducted, and the MEC value is estimated as an indicator of photoreactivity. Since MEC values cannot be calculated for complex plant extracts, an alternative evaluation method is required for evaluating photoexcitability of plant extracts by UV/VIS spectral analysis.

The present study was focused on mass percent concentration and UV/VIS absorbance of ingredients. In the IFRA standards booklet, limit concentrations of some cosmetic ingredients in finished products have been reported on the basis of sensitization and phototoxicity data. Since the limit concentration of cosmetic ingredients represents the practical maximum, accumulation of the data on absorbance of phototoxic ingredients at their limit concentration would be useful for setting absorbance criteria in UV/VIS

Table 1
Maximum UV/VIS absorption values of plant extracts at limit concentrations.

No.	Sample name	CAS No.	Limit concentration[a] (%)	Maximum UV/VIS absorption [Wavelength (nm)]	
Phototoxic plant extracts					
1	Angelica root oil	8015-64-3	0.8	>3	[290]
2	Bergamot oil	8007-75-8	0.4	>3	[308]
4	Cumin seed oil	8014-13-9	0.4	>3	[315]
5	Grapefruit oil	8016-20-4	4	>3	[319]
6	Lemon oil	8008-56-8	2	1.23	[290]
7	Lime oil	8008-26-2	0.7	>3	[290]
10	Tagetes oil	91722-29-1	0.01	1.18	[290]
11	Verbena oil	8024-12-2	0.2	2.02	[290]
Phototoxic chemicals					
13	5-Methoxypsoralen	484-20-8	0.0015	1.08	[310]
22	Methyl β-naphthyl ketone	93-08-3	0.2	>3	[290]
23	Methyl *N*-methylanthranilate	85-91-6	0.1	>3	[352]

[a] IFRA standards (IFRA, 2013).

spectral analysis for photosafety assessment. On the basis of the IFRA standards, 8 phototoxic plant extracts were selected, and UV/VIS spectral analysis of the extracts was conducted at their limit concentrations (Table 1). The limit concentrations of angelica root oil (**1**), bergamot oil (**2**), cumin seed oil (**4**), grapefruit oil (**5**), lemon oil (**6**), lime oil (**7**), and tagetes oil (**10**) have been reported to be 0.8%, 0.4%, 0.4%, 4%, 2%, 0.7%, and 0.01%, respectively, and their limit concentrations were employed for the UV/VIS spectral analysis. The limit concentration of verbena oil has not been set, since verbena oil (**11**) is classified as a prohibited chemical owing to its potent sensitization and phototoxicity. On the other hand, verbena absolute is classified as a restricted chemical, and its limit concentration in finished products has been set at 0.2%; therefore, in this study, the limit concentration of verbena absolute (0.2%) was employed as a limit concentration of verbena oil (**11**) for evaluating UV/VIS absorption properties. The maximum values of absorbance of the tested plant extracts in the UVB region were all over 1.0. To acquire UV/VIS absorbance data on phototoxic cosmetic ingredients at their limit concentrations, UV/VIS spectral analysis of 3 phototoxic chemicals was also conducted (Table 1). According to the IFRA standards, the limit concentrations of 5-methoxypsoralen (**13**), methyl β-naphthyl ketone (**22**), and methyl *N*-methylanthranilate (**23**) are 0.0015%, 0.2%, and 0.1%, respectively. The UV/VIS spectra (data not shown) of 5-methoxypsoralen (**13**) and methyl β-naphthyl ketone (**22**) showed maximum absorbance values of 1.08 and over 3 in the UVB region, respectively, while methyl *N*-methylanthranilate (**23**) showed a maximum absorption value of over 3 in the UVA region. The absorbance values of all tested ingredients at their limit concentrations were at least 1.0, and the tested ingredients at their limit concentrations have low phototoxic potential on the basis of the IFRA standards; thus, plant extracts may not have phototoxic potential if their values of absorbance are less than 1.0 in UV/VIS spectral analysis at the concentrations used in the finished products. Herein, a UV/VIS absorbance of 1.0 was set as a tentative criterion for the UV/VIS spectral analysis of plant extracts.

3.2. ROS and mROS assays

In the validated protocol of the ROS assay (Onoue et al., 2013b, 2014), a test chemical concentration of 200 μM was used for monitoring ROS generation under simulated sunlight exposure. This is not applicable to complex cosmetic ingredients, and an alternative concentration unit is required for undertaking ROS assay for plant extracts. In this study, mass concentration (μg/mL) was selected as a concentration unit, and an appropriate concentration of test substances for the ROS assay was explored. To set the assay concentration, the molecular weight distribution of 34 phototoxic chemicals was surveyed on the basis of the previous investigation, as shown in Fig. 1 (Onoue et al., 2013a). The mode value in the molecular weight distribution was in the range of 200–300 (12 chemicals), and a value of 250 was selected as a tentative average molecular weight of phototoxic chemicals in complex cosmetic ingredients. On this basis, a mass concentration of 50 μg/mL would be equivalent to a molar concentration of 200 μM, and thus, ROS and mROS assays with 50 μg/mL concentration of test substances was examined for evaluation of photoreactivity. To clarify the predictive capacity of the ROS assay systems at the set assay concentration, ROS generation from 29 phototoxic and 17 non-phototoxic chemicals used in the previous report (Onoue et al., 2013a) was examined by ROS or mROS assay at the concentration of 50 μg/mL (Table 2). The photoreactivity of the tested substances (50 μg/mL) was categorized by using the criteria of ROS generation from 200 μM chemicals reported previously [singlet oxygen: 25 ($\Delta A_{440nm} \times 10^3$); and superoxide: 20 ($\Delta A_{560nm} \times 10^3$)] (Onoue et al., 2008). On the basis of the ROS data obtained, all phototoxic chemicals exhibited potent singlet oxygen and/or superoxide generation under simulated sunlight exposure, and they were correctly determined to be photoreactive agents. As for 17 non-phototoxic chemicals, 12 chemicals (ca. 70.6%) were categorized to be non-photoreactive agents on the basis of the criteria, and 5 false-positive predictions (ca. 29.4%) [3-(4-methylbenzylidene) camphor (**52**), ascorbic acid (**53**), lauric acid (**58**), methyl salicylate (**65**), and penicillin G (**66**)] were obtained. These photoreactive outcomes on tested chemicals at 50 μg/mL were in broad agreement with those at 200 μM (Onoue et al., 2013a); the specificity and sensitivity of the ROS assay systems under the present conditions were calculated to be 85.3% and 100%, respectively. These results would indicate that the ROS/mROS assays for substances at the concentration of 50 μg/mL would have favorable predictive capacity, and this assay concentration may be acceptable for evaluating the photoreactivity of complex cosmetic ingredients by means of ROS and mROS assays.

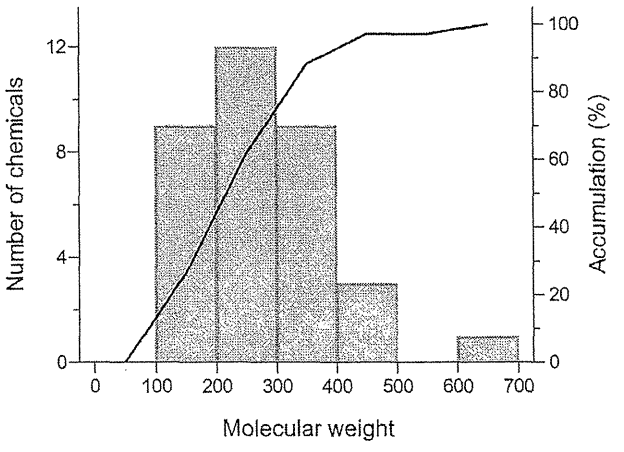

Fig. 1. Molecular weight distribution of 34 phototoxic chemicals. Column, number of chemicals; solid line, cumulative curve.

To confirm the applicability of the ROS assay to complex cosmetic ingredients, ROS generation from 11 phototoxic and 9 non-phototoxic plant extracts (50 μg/mL) was examined (Table 2). Potent generation of ROS, mainly singlet oxygen, from all phototoxic plant extracts was observed, and all phototoxic ingredients were correctly determined to be photoreactive. As regards non-phototoxic ingredients, 5 plant extracts were categorized correctly, though 4 non-phototoxic ingredients exhibited ROS generation, resulting in false-positive predictions. The specificity and sensitivity of the ROS assay for the tested plant extracts were estimated to be 73.3% and 100%, respectively. No false-negative prediction was observed in the ROS assay for plant extracts although false positive rate of the ROS assay was calculated to be ca. 44.4%; therefore, upon the present findings, the ROS assay at 50 μg/mL would have acceptable prediction capacity for photoreactivity of complex cosmetic ingredients. Further accumulation of ROS data for complex cosmetic materials would be of help for clarifying applicability of ROS assay at 50 μg/mL.

3.3. 3T3 NRU PT

3T3 NRU PT was validated under the auspices of European Centre for the Validation of Alternative Methods (ECVAM) as an *in vitro* alternative methodology to *in vivo* phototoxicity tests (Liebsch and Spielmann, 2002), and the test has been accepted by the European Union commission and member states as being necessary for all compounds showing absorbance of UV/VIS light

Table 2
ROS data for 20 plant extracts and 46 chemicals.

No.	Sample name	CAS No.	ROS data[a]			
			50 μg/mL			200 μM[b]
			Singlet oxygen ($\Delta A_{440nm} \cdot 10^3$)	Superoxide ($\Delta A_{560nm} \cdot 10^3$)	Judgment[c]	Judgment[c]
Phototoxic materials						
Plant extracts						
1	Angelica root oil	8015-64-3	43 ± 2	<1	+	
2	Bergamot oil	8007-75-8	67 ± 15	<1	+	
3	Celery seed oil	8015-90-5	28 ± 10	<1	+	
4	Cumin seed oil	8014-13-9	44 ± 17	18 ± 3	+	
5	Grapefruit oil	8016-20-4	34 ± 2	<1	+	
6	Lemon oil	8008-56-8	84 ± 6	<1	+	
7	Lime oil	8008-26-2	35 ± 1	<1	+	
8	Oil parsley	8000-68-8	31 ± 2	20 ± 2	+	
9	St. John's wort powder		48 ± 5	<1	+	
10	Tagetes oil	91722-29-1	104 ± 2	<1	+	
11	Verbena oil	8024-12-2	37 ± 5	<1	+	
Cosmetics						
12	4-Methyl-7-ethoxycoumarin	87-05-8	580 ± 23	127 ± 2	+	+
13	5-Methoxypsoralen	484-20-8	241 ± 35	63 ± 26	+	+
14	6-Methylcoumarin	92-48-8	155 ± 13	146 ± 9	+	+
15	7-Methoxylcoumarin	531-59-9	799 ± 21	4 ± 15	+	+
16	8-Methoxypsoralen	298-81-7	63 ± 10	109 ± 5	+	+
17	Benzophenone	119-61-9	201 ± 15	55 ± 11	+	+
18	Bithionol	97-18-7	162 ± 3	74 ± 6	+	+
19	Dichlorophene	97-23-4	161 ± 16	<1	+	+
20	Fenticlor	97-24-5	171 ± 3	<1	+	+
21	Hexachlorophene	70-30-4	384 ± 8	17 ± 12	+	+
22	Methyl β-naphthyl ketone	93-08-3	870 ± 15	235 ± 24	+	+
23	Methyl *N*-methylanthranilate	85-91-6	267 ± 18	<1	+	+
24	Musk ambrette	83-66-9	289 ± 16	<1	+	+
25	Musk ketone	81-14-1	192 ± 16	<1	+	+
26	Musk xylene	81-15-2	336 ± 11	<1	+	+
27	*p*-Phenylenediamine	106-50-3	<1	230 ± 10	+	+
28	Triclocarban	101-20-2	25 ± 16	<1	+	+
Non-cosmetics						
29	Acridine	260-94-6	238 ± 19	282 ± 10	+	+
30	Amiodarone HCl	19774-82-4	248 ± 8	<1	+	+
31	Chlorpromazine HCl	69-09-0	71 ± 8	67 ± 4	+	+
32	Diclofenac Na	15307-79-6	338 ± 6	420 ± 21	+	+
33	Enoxacin	74011-58-8	408 ± 2	298 ± 5	+	+
34	Fenofibrate	49562-28-9	763 ± 20	<1	+	+
35	Indomethacin	53-86-1	26 ± 10	120 ± 6	+	+
36	Ketoprofen	22071-15-4	759 ± 18	119 ± 3	+	+
37	Piroxicam	36322-90-4	183 ± 25	234 ± 21	+	+
38	Promethazine HCl	58-33-3	133 ± 17	46 ± 8	+	+
39	Sulfanilamide	63-74-1	244 ± 35	350 ± 13	+	+
40	Tetracycline HCl	64-75-5	245 ± 12	164 ± 6	+	+
Non-phototoxic materials						
Plant extracts						
41	Carrot oil	8015-88-1	<1	1 ± 8	–	
42	Corn oil	8001-30-7	1 ± 5	35 ± 34	+	
43	Ginger oil	8007-08-7	35 ± 19	3 ± 10	+	
44	Lemongrass oil	8007-02-1	49 ± 3	23 ± 18	+	
45	Olive oil	8001-25-0	7 ± 2	12 ± 3	–	
46	Orange oil	8008-57-9	94 ± 3	<1	+	
47	Rape seed oil	8002-13-9	13 ± 2	7 ± 4	–	
48	Safflower oil	8001-23-8	1 ± 3	4 ± 4	–	
49	Soybean oil	8001-22-7	<1	<1	–	
Cosmetics						
50	1,3-Butylene glycol	107-88-0	7 ± 4	<1	–	–
51	2-Propanol	67-63-0	<1	3 ± 3	–	–
52	3-(4-Methylbenzylidene)camphor	36861-47-9	213 ± 10	<1	+	–
53	Ascorbic acid	50-81-7	368 ± 10	199 ± 4	+	+
54	Cetyl alcohol	36653-82-4	<1	<1	–	–
55	Ethanol	64-17-5	<1	7 ± 1	–	–
56	Glycerine	56-81-5	6 ± 1	<1	–	–
57	Isopropyl myristate	110-27-0	5 ± 6	<1	–	–
58	Lauric acid	143-07-7	16 ± 1	23 ± 1	+	–
59	Propylene glycol	57-55-6	11 ± 4	<1	–	–
60	Sodium laurate	629-25-4	6 ± 0	<1	–	–
61	Sodium lauryl sulfate	151-21-3	<1	<1	–	–
62	Sulisobenzone	4065-45-6	<1	<1	–	–

Table 2 (*continued*)

No.	Sample name	CAS No.	ROS data[a]			
			50 μg/mL			200 μM[b]
			Singlet oxygen ($\Delta A_{440nm} \cdot 10^3$)	Superoxide ($\Delta A_{560nm} \cdot 10^3$)	Judgment[c]	Judgment[c]
Non-cosmetics						
63	DMSO	67-68-5	<1	12 ± 1	–	–
64	Lactic acid	50-21-5	7 ± 2	<1	–	–
65	Methyl salicylate	119-36-8	<1	26 ± 8	+	+
66	Penicillin G	61-33-6	1 ± 12	30 ± 7	+	–

[a]Plain letters: ROS data from ROS assay in clear solution; plain letters in open box: ROS data from ROS assay in partial suspension; and plain letters in gray box: ROS data from mROS assay.
[b]Onoue et al. (2013a).
[c]+, positive; and –, negative.

Table 3
Photochemical and phobiochemical data for tested plant extracts.

No.	Sample name	Maximum UV/VIS absorption[a]	ROS data		PIF value
			Singlet oxygen ($\Delta A_{440nm} \cdot 10^3$)	Superoxide ($\Delta A_{560nm} \cdot 10^3$)	
Phototoxic plant extracts					
1	Angelica root oil	>3	43	<1	1.1
2	Bergamot oil	>3	67	<1	2.0
3	Celery seed oil	–	28	<1	1.2
4	Cumin seed oil	>3	44	18	6.4
5	Grapefruit oil	>3	34	<1	1.0
6	Lemon oil	1.23	84	<1	1.0
7	Lime oil	>3	35	<1	1.0
8	Oil parsley	–	31	20	1.1
9	St. John's wort powder	–	48	<1	83.8
10	Tagetes oil	1.18	104	<1	47.7
11	Verbena oil	2.02	37	<1	1.1
Non-phototoxic plant extracts					
41	Carrot oil	–	<1	1	1.0
42	Corn oil	–	1	35	1.0
43	Ginger oil	–	35	3	1.0
44	Lemongrass oil	–	49	23	1.5
45	Olive oil	–	7	12	1.0
46	Orange oil	–	94	<1	1.2
47	Rape seed oil	–	13	7	1.0
48	Safflower oil	–	1	4	1.0
49	Soybean oil	–	<1	<1	1.0

[a] –: not conducted because no limit concentration is given in IFRA standards (IFRA, 2013).

(Onoue et al., 2009). Therefore, 3T3 NRU PT using the Balb/c 3T3 mouse fibroblast cell line was conducted for 20 plant extracts in the present study (Table 3). 3T3 NRU PT assesses the cytotoxic effects of a chemical with and without UVA irradiation at a non-cytotoxic dose, and the PIF value is calculated on the basis of the IC_{50} values with and without UV irradiation. The OECD test guideline 432 classifies materials into three groups, according to PIF value: (i) non-phototoxic materials (PIF < 2), (ii) probably phototoxic materials ($2 \leqslant PIF < 5$), and (iii) phototoxic materials ($PIF \geqslant 5$). In the cases of St. John's wort powder (**9**) and tagetes oil (**10**), the UVA-irradiated groups showed much lower IC_{50} values than the non-irradiated groups, and their PIF values were estimated to be 83.8 and 47.7, respectively. The IC_{50} values of irradiated bergamot oil (**2**) and cumin seed oil (**4**) were also lower than those of non-irradiated groups, and their PIF values were calculated to be 2.0 and 6.4, respectively. Thus, according to the classification criteria, cumin seed oil (**4**), St. John's wort powder (**9**), and tagetes oil (**10**) were considered to be phototoxic, and bergamot oil (**2**) was determined to be probably phototoxic. In contrast, other phototoxic plant extracts and all non-phototoxic ones were identified as non-phototoxic, since no significant difference was observed in cell viability curves between UV-irradiated and non-irradiated groups, providing PIF values of less than 2. Thus, most of the phototoxic plant extracts were falsely judged as negative. This result is in agreement with previous reports for three phototoxic ingredients: angelica root oil (**1**), lemon oil (**6**) and grapefruit oil (**5**) (Okamoto et al., 2002; Okamoto, 2005). These phototoxic plant extracts had also shown no photoirritant reaction in previous *in vivo* phototoxicity testing; therefore, the present results from the 3T3 NRU PT are consistent with the outcomes of *in vivo* phototoxicity tests. UV/VIS spectral analysis and ROS assay can predict photoreactivity of complex cosmetic ingredients; however, photoreactive events do not always result in phototoxic reactions, and so other *in vitro* phototoxicity tests based on photobiochemical reactions are needed for detailed photosafety assessment of cosmetic ingredients. Thus, 3T3 NRU PT would be useful as a follow-up assay to predict phototoxic risk of photoreactive ingredients.

3.4. Proposed testing approach for complex cosmetic ingredients

3.4.1. Screening approach

In the present study, the photosafety of 20 plant extracts was assessed by means of modified *in vitro* photochemical and photobiochemical assays, the strategic use of which has already been proposed for photosafety testing of pharmaceutical substances in

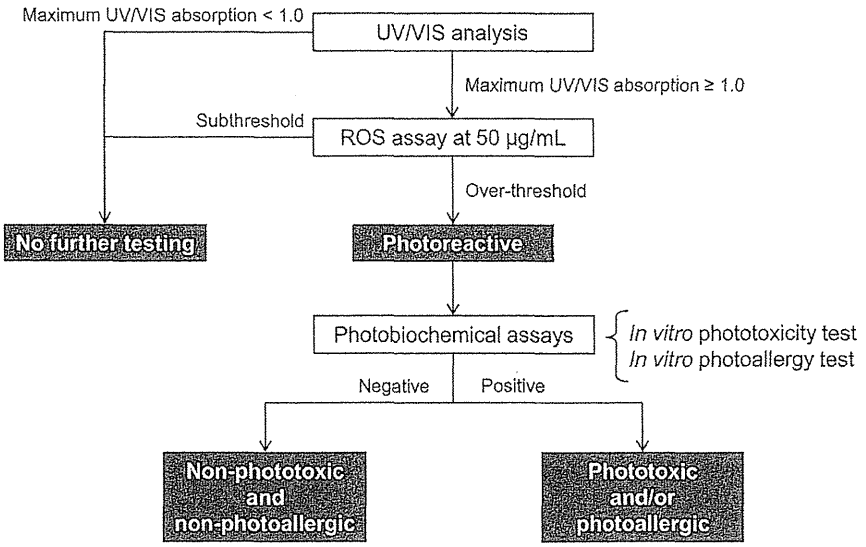

Fig. 2. Proposed *in vitro* photosafety evaluation scheme for complex cosmetic ingredients.

the ICH S10 guideline (ICH, 2014) and of cosmetic ingredients in the previous study (Onoue et al., 2013a). Since complex cosmetic ingredients do not have specific molecular weights, modifications of the assay procedures and decision criteria are needed for photosafety assessment of these ingredients. On the basis of the outcomes from the present study, a tiered testing approach was proposed for non-animal photosafety assessment of complex cosmetic ingredients (Fig. 2).

Since absorption of UV/VIS light by phototoxins would be a key trigger of phototoxic/photoallergic events, UV/VIS spectral analysis using maximum UV absorption values should be available for initial screening. In the present study, the limit concentrations described in IFRA standards were employed as test sample concentrations in UV/VIS spectral analysis, and the maximum UV/VIS absorption values of all tested phototoxic samples were over 1.0. According to IFRA standards, material at its limit concentration is safe as regards phototoxicity, and thus, the maximum UV/VIS absorption value of 1.0 was chosen as a tentative criterion for photosafety identification of complex cosmetic ingredients. Then, ROS assay is applied to all ingredients with a maximum UV/VIS absorption value over 1.0. In the ROS assay, the 50 μg/mL concentration of test samples was employed, and obtained no false-negative prediction. Therefore, ROS assay at 50 μg/mL appears to be suitable for photoreactivity evaluation of complex cosmetic ingredients. If the tested ingredients were not photoreactive in the ROS assay, no further testing would be needed. Potent ROS generators would need to be further assessed with photobiochemical assessment tools in order to identify their phototoxic mechanisms in detail since false-positive predictions were provided with high rate. Thus, 3T3 NRU PT would be useful as a follow-up photobiochemical assay for evaluating *in vitro* phototoxicity. When a tested complex cosmetic ingredient is judged as positive in photobiochemical assays, its use as a cosmetic ingredient cannot be recommended.

3.4.2. Limitations of the proposed photosafety approach

Although the proposed overall photosafety approach appears to be effective on the basis of the obtained data, there are some limitations in the individual assessment tools. In the UV/VIS spectral analysis, the maximum UV/VIS absorption value was employed as an alternative judgment factor to the MEC value; however, the scale of the obtained absorption data was quite small in the present investigation, and therefore it still needs to be confirmed that the maximum UV/VIS absorption value is a reliable judgment factor. Thus, accumulation of substantial maximum UV/VIS absorption data and photosafety information on complex cosmetic ingredients may allow us to identify a different threshold with better predictivity. As for the ROS assay at 50 μg/mL, this showed an acceptable predictive ability for evaluating photosafety of complex cosmetic ingredients. On the other hand, ROS assay has solubility issues and false-positive prediction as assay limitations (Onoue et al., 2013b), and, in fact, the high rate of false-positive prediction was one of the issues in the present study. Further, complex cosmetic ingredients contain various chemicals, and photochemical interactions among these constituents might occur in assay mixtures. In addition, redox reactions involving reduced and/or peroxy chemicals might interfere with the detection of ROS generation based on oxidative reactions of probes. Such interactions may lead to false predictions. 3T3 NRU PT can mainly evaluate photoirritancy risk of chemicals (Onoue et al., 2009), and cannot detect some photoallergic ingredients (SCCS, 2012). Furthermore, cytotoxic UVB radiation is generally filtered out during the assay to avoid death of Balb/c 3T3 mouse fibroblast cells. Hence, photoallergic materials and UVB absorbers tend to be falsely evaluated as non-phototoxic ingredients by 3T3 NRU PT. In regards to photoallergy potential, the use of *in vitro* photoallergic risk assessment tools would be required for reliable photosafety assessments. Recently, a photo human Cell Line Activation Test (photo-h-CLAT) (Hoya et al., 2009; Hino et al., 2008) has been reported, and this might be helpful for photosafety screening. Overall, although there are some limitations of *in vitro* photosafety tests, these findings would indicate that the proposed strategic approach can be effective for non-animal photosafety assessment of complex cosmetic ingredients.

4. Conclusion

The present study has demonstrated the applicability of modified *in vitro* photochemical assessment tools, including UV/VIS spectral analysis and ROS assay to complex cosmetic ingredients. On the basis of the present results, acceptable modifications of procedures in *in vitro* photochemical assessment tools might be helpful for development of photosafety assessment strategy for complex cosmetic ingredients; however, the low reliability of the